

A&A manuscript no.

(will be inserted by hand later)

Your thesaurus codes are:

08.06.3; 08.08.1; 10.15.1; 10.15.2 Orion OB1; 09.02.1

ASTRONOMY
AND
ASTROPHYSICS
15.7.2018

The Orion OB1 association *

I. Stellar content

A.G.A. Brown¹, E.J. de Geus^{2,3} and P.T. de Zeeuw¹

¹ Sterrewacht Leiden, P.O. Box 9513, 2300 RA, Leiden, The Netherlands

² Astronomy Department, Caltech, Pasadena, CA 91125, USA

³ Astronomy Department, University of Maryland, College Park, MD 20742, USA

Received..., accepted...

Abstract. Walraven photometry of established and probable members of the Orion OB1 association is presented. Effective temperature, surface gravity, luminosity and mass are derived for all stars, using atmosphere models by Kurucz (1979). Absolute magnitudes are calculated using the Straizys and Kuriliene (1981) tables. Distance moduli and visual extinctions are determined. A comparison of the visual extinctions to IRAS 100 μm data shows that the near edge of the Orion A and B clouds lies at a distance of ~ 320 pc, while the far edge is at ~ 500 pc. A method for deriving the ages of the subgroups by comparing theoretical isochrones to the observations in the $\log g$, $\log T_{\text{eff}}$ plane is presented. The derived ages suggest, contrary to earlier studies, that subgroup 1b is younger than 1c, which can possibly be explained by past geometries of the system of stars and gas. The initial mass function for Orion OB1 is derived with the aid of the Kolmogorov-Smirnoff test. Through extensive simulations, we show that it is very difficult to derive accurately the IMF from the available data. To within somewhat weak limits the IMF is found to be of the form $\xi(\log M) = AM^{-1.7 \pm 0.2}$ for all subgroups. The energy output of the subgroups in the form of stellar winds and supernovae is calculated and compared to the observed size and expansion velocity of the Orion-Eridanus bubble. It is shown that the energy output of the association can account for the morphology and kinematics of the ISM.

Key words: stars: fundamental parameters – Hertzsprung-Russell diagram – open clusters and associations: general, individual: Orion OB1 – ISM: bubbles

Send offprint requests to: A.G.A. Brown

* Based on *VBLUW* Photometry obtained with the 91-cm Dutch Telescope at ESO, La Silla

1. Introduction

OB associations play an important role in the large scale propagation of star formation and in the shaping and evolution of the interstellar medium. The OB star complex in Orion is an excellent laboratory for an investigation of these processes. It contains the four subgroups of the Orion OB1 association as well as the Orion Molecular Cloud (OMC) which is one of the nearest sites of active OB star formation. The subgroups were identified by Blaauw (1964), and differ in age and in content of gas and dust. The different evolutionary phases of the subgroups make the Orion region well suited for studying the influence of OB associations on the surrounding interstellar medium and for constraining scenarios of sequential star formation, such as suggested by Elmegreen & Lada (1977). Knowledge of the stellar content also provides clues to the origin of the initial mass function.

The stars in Orion OB1 have been studied by a number of authors (see Blaauw 1964; Genzel & Stutzki 1989). Early photometric and spectroscopic work by Parenago (1954) and Sharpless (1952, 1962) was followed by the massive investigation by Warren & Hesser (1977, 1978, hereafter WH) based on *uvwby* photometry. These authors derived distances and ages for the subgroups. Proper motion investigations were carried out by Parenago (1953), Strand (1958), Lesh (1968) and more recently by Van Altena et al. (1988), Jones & Walker (1988) and Smart (1993).

The interstellar medium near Orion OB1 contains several large scale features, including H α emission extending to Eridanus, partly observable as Barnard's loop, and a hole in the H I distribution, which is surrounded by expanding shells (Goudis 1982). Reynolds & Ogden (1979) and Cowie et al. (1979) argued that the coherent gas motions in Orion are the result of a series of supernova events which took place up to 4×10^6 yr ago, but they ignored the

effects of stellar winds. In the past fifteen years a wealth of new data has been gathered on the large scale interstellar medium in Orion, through surveys in ^{12}CO (Maddalena et al. 1986), ^{13}CO (Bally et al. 1987), CS (Lada et al. 1991), the far-infrared (IRAS sky survey) and HI (Chromey et al. 1989; Green 1991; Green & Padman 1993; Hartmann & Burton 1993). At the same time, the theory of stellar winds has been developed to the extent that their impact on the surrounding medium can now be readily estimated (Kudritzki et al. 1989; McCray & Kafatos 1987; de Geus 1991, 1992). A new investigation of the stellar content of the Orion OB1 association, especially in relation to the large scale structures in the surrounding ISM, is therefore justified and timely.

This paper is organized as follows. The next section describes the sample of stars and the photometric observations. In section 3 the method used for deriving physical parameters of the stars ($\log g$ and $\log T_{\text{eff}}$) from *VBLUW* photometry is summarized. Section 4 describes a number of properties of the stellar content of the Orion OB1 association. These include ages and distances of the subgroups, derivation of membership criteria, correlations between the visual extinctions of the stars and gas and dust around the association (using IRAS skyflux data) and a calculation of mass functions and the energy output of the subgroups in Orion OB1. The relation between the stars and the large scale structures in the surrounding ISM is described in section 5. Section 6 contains the conclusions and suggestions for future work.

2. Observations

The stars studied in this paper are established or probable members of the Orion OB1 association.

In order to obtain a list of potential members down to spectral type F, the CSI catalogue (Jung & Bischoff 1971) was searched with a number of selection criteria. The coordinates were limited by: $196^{\circ} \leq \ell \leq 217^{\circ}$, and $-27^{\circ} \leq b \leq -12^{\circ}$ (Blaauw 1964). All O and B stars in this area were selected, while A and F stars were required to have $m_B \geq 7^m$, respectively $m_B \geq 9^m$, to avoid a large number of foreground objects. The CSI catalogue is complete down to $m_V \approx 9^m$, and is limited at $m_V \approx 12^m$. This selection procedure resulted in 1318 stars, which were included in a 1982 HIPPARCOS proposal to observe all OB associations within 800 pc from the Sun.

Photometric observations were carried out between 1982 and 1989 with the 91-cm Dutch telescope at ESO, in the *VBLUW* Walraven system (Lub & Pel 1977; de Geus, de Zeeuw & Lub 1989, hereafter GZL). This provided measurements for 986 of the 1318 stars, tabulated by de Geus et al. (1990). These stars are the subject of this paper. The mean rms errors in the observed intensities are: $\bar{\sigma}(V) = 0.0016$, $\bar{\sigma}(V - B) = 0.0010$, $\bar{\sigma}(B - U) = 0.0012$, $\bar{\sigma}(U - W) = 0.0015$, $\bar{\sigma}(B - L) = 0.0012$. Multiplication

by 2.5 provides the mean rms errors in magnitudes. The stars were divided in two categories: 373 priority 1 stars which are a) stars of spectral type O and B, and/or b) stars that are established or probable members of the association according to WH, who used proper motion data, radial velocities and *UBV* as well as *uvby* photometric observations. The remaining 613 stars have priority 2.

The final HIPPARCOS Input Catalog contains 699 stars of our original sample of 1318 stars in Orion OB1, of which 236 are priority 1, and 463 are priority 2.

3. Derivation of physical parameters

The derivation of physical parameters from photometric data involves a number of steps in which theoretical and empirical transformations are used. We follow the procedure used by GZL in their study of Sco OB2.

The first step is the calculation of reddening-independent colours. In the Walraven system these are defined as (Lub & Pel 1977):

$$\begin{aligned} [B - U] &= (B - U) - 0.61(V - B) , \\ [U - W] &= (U - W) - 0.45(V - B) , \\ [B - L] &= (B - L) - 0.39(V - B) . \end{aligned} \quad (1)$$

The colour $(V - B)$ essentially measures the reddening, $[B - U]$ is an indicator of $\log T_{\text{eff}}$, and for O and B stars $[U - W]$ and $[B - L]$ each depend mostly on $\log g$. The errors in the reddening-independent colours are caused by observational errors and by possible local variations in the value R of total to selective extinction. WH find that a normal reddening law is appropriate for Orion OB1, except for selected regions such as the Orion Nebula. We have therefore adopted the conventional value $R = 3.2$. This is reflected in the coefficients of Eq. (1).

The next step is the determination of effective temperature and surface gravity. These were derived from the reddening-independent colours by employing a grid of theoretical colours for a wide range of T_{eff} and $\log g$, obtained by convolution of the Kurucz (1979) atmosphere models with the Walraven passbands. The availability of three reddening-independent colours allows the construction of two independent reddening-free colour-diagrams; $[B - U]$ vs. $[U - W]$ and $[B - U]$ vs. $[B - L]$. Due to uncertainties in the calibration of the Kurucz grid in the $[B - U]$ vs. $[U - W]$ plane (Brand & Wouterloot 1988), only the $[B - U]$ vs. $[B - L]$ diagram was used. Figure 1 shows the Kurucz grid in this diagram together with all our programme stars. The values of $\log T_{\text{eff}}$ and $\log g$ were determined by two-dimensional linear interpolation in the grid. The Kurucz models are unreliable for stars with $T_{\text{eff}} < 8000\text{K}$, and we therefore excluded all stars with $[B - U] < 0.3$ and $[B - L] > 0.13$. Stars with $\log g \geq 4.5$ just outside the grid were assigned $\log g$ and $\log T_{\text{eff}}$ by taking into account their observational errors, or by using an extrapolation of the grid as described by Brand

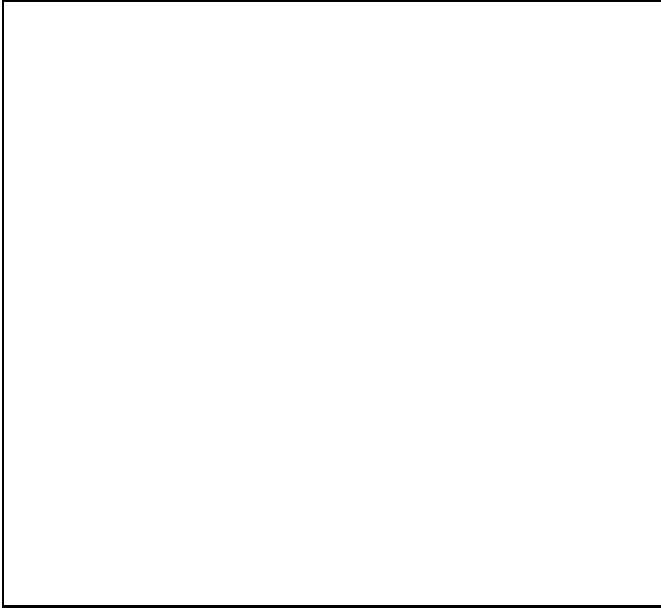


Fig. 1. The Kurucz grid in the reddening-independent two-colour diagram of $[B - U]$ vs. $[B - L]$. Solid lines indicate constant $\log T_{\text{eff}}$ and dashed lines constant $\log g$. Values of $\log T_{\text{eff}}$ and $\log g$ are indicated. Points are the observations for our sample of stars in Orion

& Wouterloot (1988). Other stars outside the grid were excluded. A number of stars lie in the part of the diagram where the Kurucz grid folds over itself, resulting in multiple solutions. These were checked carefully by investigating the extinctions (which have to be positive) and by comparing temperatures and spectral types. Usually only one solution remained and $\log g$ and $\log T_{\text{eff}}$ could be assigned. The errors in the derived $\log T_{\text{eff}}$ and $\log g$ are due to the propagation of errors in the original input-colours and to systematic errors in the Kurucz grid. The errors in the grid are largest for temperatures above 25000 K (and below 8000 K). This results in $\bar{\sigma}(\log T_{\text{eff}}) \approx 0.015$ for $\log T_{\text{eff}} < 4.3$ and $\bar{\sigma}(\log T_{\text{eff}}) \approx 0.03$ for $\log T_{\text{eff}} \geq 4.3$. The errors in $\log g$ are ≈ 0.1 and ≈ 0.25 , respectively.

The absolute visual magnitude M_V and the absolute bolometric magnitude M_{bol} were derived from $\log T_{\text{eff}}$ and $\log g$ by means of the calibration Tables of Straizys & Kuriliene (1981). These give $\log T_{\text{eff}}$, $\log g$, M_V , M_{bol} , spectral type and luminosity class, based on a combination of empirical calibrations and theoretical calculations. We employed two-dimensional linear interpolation in these Tables to derive M_V and M_{bol} . The luminosity was calculated from the bolometric magnitude by:

$$\log \frac{L}{L_{\odot}} = -0.4M_{\text{bol}} + 1.888. \quad (2)$$

As can be seen in Fig. 2 of GZL, the Kurucz grid and the Straizys & Kuriliene calibrations do not overlap entirely. This implies that a number of stars have $\log g$, $\log T_{\text{eff}}$ solutions from the Kurucz grid, but can not be

assigned a magnitude. For stars on the main-sequence, but with $\log g$ values just below the ZAMS line in Fig. 2 of GZL, we used $\log T_{\text{eff}}$ to assign a photometric spectral type. The luminosity class was determined by assuming that stars with $T_{\text{eff}} \geq 25000$ K are of luminosity class V. The other main-sequence stars were assigned luminosities corresponding to a ZAMS star in the Tables of Straizys & Kuriliene. The absolute magnitude of a star is very sensitive to both T_{eff} and $\log g$, so that the errors in derived temperature and gravity cause large uncertainties in the values of M_V and M_{bol} . We estimate $\bar{\sigma}(M_{\text{bol}}) \approx 0^m3$.

The Kurucz grid can also be used in observed-colour space to transform $\log T_{\text{eff}}$ and $\log g$ to the intrinsic colours. The colour excess in the Walraven system, $E_{(V-B)}$ is the difference of the observed colour ($V - B$) and the intrinsic colour $(V - B)_0$: $E_{(V-B)} = (V - B) - (V - B)_0$. The colour excess in the Johnson system, $E_{(B-V)}$, follows from that in the Walraven system by (GZL):

$$E_{(B-V)} = 2.39E_{(V-B)} - 0.17E_{(V-B)}^2. \quad (3)$$

The total visual extinction A_V is then given by $A_V = 3.2E_{(B-V)}$.

To determine the distance modulus of a star we need the apparent visual magnitude m_V in the Johnson system, because the Straizys & Kuriliene calibrations give the absolute magnitude in this system. The following transformation formula was used to derive m_V from the Walraven V and $(V - B)$ (GZL):

$$m_V = 6.886 - 2.5V - 0.082(V - B). \quad (4)$$

The distance modulus then follows from the usual relation: $5 \log D - 5 = m_V - M_V - A_V$. The mean errors in A_V and m_V are 0^m03 and 0^m015 , respectively. The error in the distance modulus is dominated by the error in M_V , and is approximately 0^m3 .

The results are presented in Table 1. The first three columns give the identification of each star: column 1 is the HD or BD number, column 2 lists the number of the star in the HIPPARCOS Input Catalogue (HIC, Turon et al. 1992), and column 3 gives the name. Columns 4–6 list $\log T_{\text{eff}}$, $\log g$ and $\log L/L_{\odot}$. Column 7 gives m_V . Column 8 lists the absolute magnitude and column 9 the visual extinction. Column 10 lists the distance modulus and column 11 gives an indication of the membership: members according to the criteria described in Section 4 have a blank, possible members based on the findings from photometry are designated with PM and non-members are denoted by NM. An asterisk in column 11 means that the star is included in Fig. 6a and a plus means that it is included in Fig. 6b (see section 4.3). Column 12 gives the spectral type according to the MK-classification, taken from the HIPPARCOS Input Catalogue. De Geus et al. (1990) give the original photometric data, the positions on the sky and the priority (1 or 2) for all the stars.

Absolute magnitudes and distance moduli for the stars HD 37022, HD 37128 and HD 38771 could not be determined because the stars lie outside the Kurucz grid or $\log g$ and $\log T_{\text{eff}}$ are outside the range of the Straizys & Kuriliene calibrations. Physical parameters for HD 37128 and HD 38771 were taken from Lamers & Leitherer (1993) and Vilkoviskij & Tambovtseva (1992), respectively.

4. Properties of the Orion OB1 association

Blaauw (1964) divided Orion OB1 into four subgroups: 1a, which contains the stars to the northwest of the Belt stars; 1b, containing the group of stars located around the Belt (including the Belt stars themselves); 1c, in which the stars around the Sword are included; and 1d, which contains the stars in and close to the Orion Nebula (including the Trapezium stars). Subgroups 1b, 1c and 1d were subdivided further in subsequent studies. WH split subgroup 1b into three parts because Hardie et al. (1964) and Crawford & Barnes (1966) found that the distance of the Belt stars increases from west to east. We also used this subdivision in the determination of membership criteria (Section 4.1), but we found no significant differences in their mean distances, and no trend with right ascension for the 1b stars as claimed by WH. So for all other purposes subgroup 1b was treated as a whole. Morgan & Lodén (1966) and Walker (1969) divided 1c into several smaller sub-groupings located close to the Orion Nebula. WH found no evolutionary differences between these groups, so we decided to treat subgroup 1c as a whole also. WH divided subgroup 1d in an outer Nebula region and an inner Nebula region, in the hope that an accurate distance modulus could be determined for the outer region which could then be applied to the inner region. We used the same subdivision for the distance determination.

4.1. Distances to the subgroups; photometric membership determination

Ideally one would use the established proper motion (and radial velocity) members of a stellar group to derive its mean distance and distance spread, and then use these to determine photometric membership for stars without measured proper motions or radial velocities. However, we would like to point out here that this procedure works well for open clusters, but that in the case of associations assigning membership based on the motions of the stars is a more complicated problem. This is due to the fact that associations are formed in a much larger region of space (of the order of tens of parsecs, the size of GMCs) and with much lower stellar space densities than open clusters. As a consequence, associations are very loose stellar aggregates in which each star is individually subject to Galactic forces. Therefore they will not stand out clearly on the sky (making it difficult to assign spatial boundaries)

or in proper motion diagrams. Furthermore, stars formed in different regions of the parental cloud might have different motions from the beginning, even if they formed at the same time. For a star at the periphery of the star forming region it will also be difficult to assign membership based on its motion: early on it might have acquired an anomalous motion as a consequence of Galactic forces. Stars in associations might also acquire anomalous motions as a consequence of supernova explosions in binaries (possibly leading to the formation of runaway stars, see e.g., Blaauw 1961) or because of dynamical ejection mechanisms (Gies & Bolton 1986, Leonard & Duncan 1988, 1990). There is also the possibility of non-coeval star formation within a subgroup, which can result in stars of different ages moving differently. In short, due to the spread in space and possibly in time of the formation of an association, the term "established proper motion member" (as derived from earlier studies) has less meaning than it has in the classical proper motion studies of open clusters. One should find better criteria (apart from, e.g., converging proper motion vectors), taking into account the formation history, for assigning membership in associations.

Nevertheless, we decided to use a subset of the stars for which WH derived membership based on proper motions, radial velocities and photometry and regard these as the established members of Orion OB1. These are the priority 1 stars in our programme and we used them to derive mean distance moduli and spreads. We used only the B stars, for which the Kurucz grid is reliable. We applied 3σ -clipping to derive the mean distance modulus, with σ being the rms spread around the mean. The results are listed in Table 2 together with the distance moduli found by WH and, for both studies, the number of stars used to derive the results. Our distance moduli are systematically smaller than those of WH, because our zero age main-sequence absolute magnitude calibration is systematically fainter than the $M_V(\beta)$ calibration used by WH. Anthony-Twarog (1982) reanalyzed the data in WH with the aid of a revised calibration of the $uvby\beta$ system (Crawford 1978). She finds distance moduli for the subgroups that are consistent with our results to within $0^m.1$. The mean distance moduli of the three subdivisions of 1b are the same within the errors. The distance to subgroup 1d is very uncertain because it is difficult to obtain accurate photometry in this highly nebulous area (the small rms spread in distance modulus is not significant, only three stars were included in the calculation of $\langle dm \rangle$).

WH based their membership assignments on proper motions, radial velocities and distance moduli. We carefully checked all the priority 1 stars with distances outside our 2σ limits. A number of these stars were marked as possible non-members by WH. While examining these stars, we took into account errors in the distance modulus, undetected duplicity, spectral peculiarities, nebulosity influence on the photometry and evolutionary effects. In this way we could exclude membership for a number of stars

Table 2. Mean distance moduli of the subgroups and rms spreads

Subgroup	WH			VBLUW		
	$\langle dm \rangle$	σ	n	$\langle dm \rangle$	σ	n
	(mag)	(mag)		(mag)	(mag)	
a	8.0	0.46	60	7.9	0.52	53
b1	8.5	0.53	14	7.8	0.39	8
b2	8.2	0.29	24	7.8	0.45	17
b3	8.0	0.55	14	7.8	0.46	6
c	8.2	0.49	78	8.0	0.49	34
d	8.4	0.53	6	7.9	0.25	3

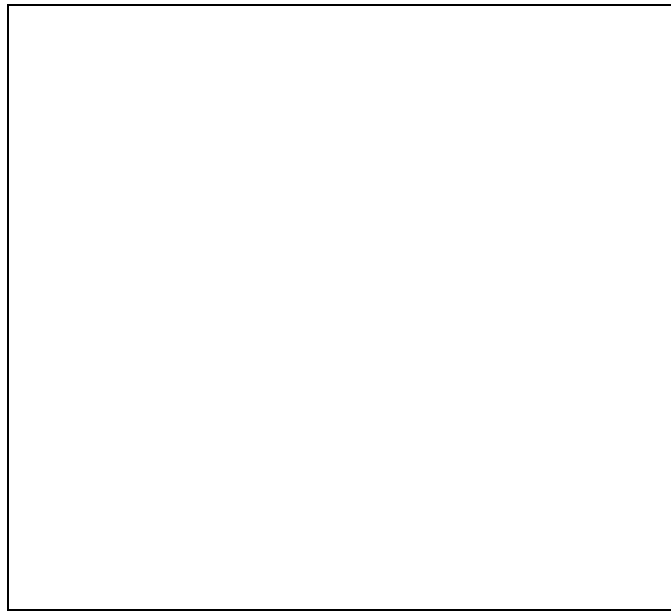


Fig. 2. Distance modulus vs. right ascension for the stars that are members of subgroup 1b

marked as doubtful members by WH. Overall we find good agreement between our membership list and that of WH.

OB associations generally have linear sizes between 10 and 100 pc (Blaauw 1991). The angular size of the Orion OB1 subgroups corresponds to sizes in the range of 20 to 45 pc, and it is likely that 100 pc is a safe upper limit to the depth of the association along the line of sight. At the distance of Orion OB1 (> 350 pc) this corresponds to $0.^m3$ intrinsic spread in the distance moduli. This means that the observational errors in the individual distance moduli are the dominant source of the spread around the mean, and that the extent of the subgroups along the line of sight cannot be resolved. The membership assignments for the priority 2 stars were therefore based on the following criteria: if the distance modulus of a star is within 2σ from the mean it is considered a member. If the star has a distance modulus that is between 2σ and 3σ from the mean it is



Fig. 3. Reddening-independent two-colour diagram for all program stars in Orion OB1. The solid line is the theoretical zero-age main-sequence

considered a possible photometric member. Otherwise it is a non-member.

The priority 2 stars in subgroups 1a and 1c cover a much larger area on the sky than the priority 1 stars in these groups. This means that selecting members only on basis of their distance modulus is likely to introduce a number of field stars in the list of members. This can never really be avoided in photometric membership determinations. For subgroup 1d we had too few stars in the outer Nebula subdivision to calculate a reliable mean distance modulus and spread. Instead we used the proper motion study of the Orion Nebula cluster (the Trapezium region) by Van Altena et al. (1988) to assign membership for all the programme stars in 1d.

In order to make our list of association members as reliable as possible we also used the proper motion data from the PPM catalogue (Röser & Bastian 1989; Bastian et al. 1991). Vector point diagrams (VPD) were constructed for the subgroups and clear outliers were excluded as members. WH obtained the following mean centennial proper motions for all subgroups: $\langle \mu_\alpha \rangle = -0.^{\circ}03 \pm 0.^{\circ}03$ and $\langle \mu_\delta \rangle = -0.^{\circ}1 \pm 0.^{\circ}5$. The mean motions found by WH are consistent with the mean motions we find for our member stars from the PPM data. The outliers in our VPD on average lie at more than $\sim 0.^{\circ}02 \text{ yr}^{-1}$ from the centroid of the subgroup, well outside the 3σ limits on the mean value of the proper motion. The errors in the PPM proper motions are $\sim 0.^{\circ}003 \text{ yr}^{-1}$. It turns out that almost all of the discarded stars are on the near side of the association between the 2σ and 3σ limits on the mean distance moduli.

As can be seen in Table 2 WH found that the distance moduli of stars in subgroup 1b increase from west to east. Figure 2 shows our distance moduli for the members of this subgroup as a function of right ascension. No trend is evident. The correlation coefficient between distance modulus and RA is 0.03 (at a significance level of 22% based on 126 data points). This result remains if we take all stars in 1b into account regardless of membership (then the correlation coefficient is -0.04 at a significance level of 32% based on 133 points). WH suggested that the trend they found could be due to the superposition of members of subgroup 1a. It is not possible to determine accurate spatial boundaries on the sky for the subgroups and our data show that 1a is located at practically the same distance as 1b. Hence, we cannot exclude the possible contamination of the membership list of 1b by 1a subgroup members.

4.2. Ages of the subgroups

Figure 3 shows the reddening-independent two-colour diagram $[B - U]$ vs. $[B - L]$ for all the programme stars together with the line representing the zero-age main-sequence (ZAMS), calculated from theoretical stellar evolution models (see below). This diagram is the observational counterpart of the $\log T_{\text{eff}}$ vs. $\log g$ diagram. Evolution causes a star to move towards the lower left corner of the diagram, so that the ZAMS is the upper right boundary of the data-points. Clearly, the bulk of our programme stars lie at or near the ZAMS. GZL describe the effects which cause a spread away from the ZAMS.

We have calculated isochrones based on the evolutionary models of Schaller et al. (1992). We restricted ourselves to models with a metallicity $Z = 0.02$, and used only the core-hydrogen-burning and the overall-contraction phases, which together cover the whole main sequence strip in the HR-diagram. The isochrones were calculated by means of the procedure described in section 4.2 of GZL.

The isochrones were used to determine the *nuclear age* of the subgroups of Orion OB1, i.e., the time it took the stars to reach their current evolutionary state measured from their arrival on the ZAMS. The accuracy of the *absolute* age determined by isochrone fitting depends on the calibration of the stellar models on which the isochrones are based. The *relative* age of different subgroups can often be determined more accurately, because the evolutionary models are internally consistent.

Isochrone fitting should preferably be done in the $[B - U]$ vs. $[B - L]$ plane, because of the high accuracy of the photometry. At the high-mass end, however, the theoretical isochrones do not overlap with the Kurucz grid. Therefore, if the subgroup contains stars with masses above $25\text{--}30 M_{\odot}$, we cannot calculate colours for isochrones covering the turn-off from the main sequence. This occurs in subgroups 1b, 1c and 1d. In this case, isochrone fitting is best done in the $\log g$, $\log T_{\text{eff}}$ plane. The values of $\log g$ and $\log T_{\text{eff}}$ for stars outside the Kurucz



Fig. 4a. Hertzsprung-Russell diagram of $\log g$ vs. $\log T_{\text{eff}}$ for subgroup 1a. The solid line is the theoretical isochrone that represents the age of the subgroup



Fig. 4b. Same as 4a for subgroup 1b

grid have been taken from detailed spectroscopic studies in the literature (section 3). Isochrone fitting in the $\log L/L_{\odot}$, $\log T_{\text{eff}}$ plane would mean the introduction of extra errors caused by the calibrations of absolute magnitude and bolometric correction. Appendix A describes the adopted fitting procedure, and the Monte Carlo simulations which were used to estimate the errors in the derived ages. These simulations include the effects of the large errors in $\log g$ and the influence of the form of the initial mass function. Chemically peculiar stars were ex-

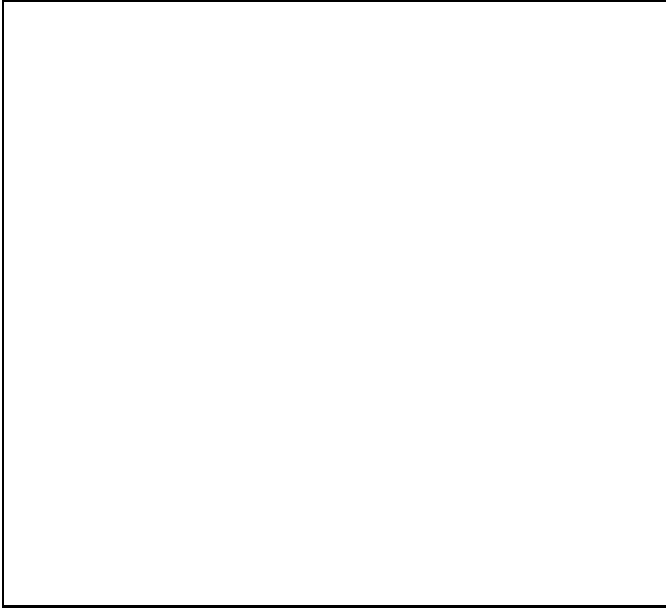


Fig. 4c. Same as 4a for subgroup 1c



Fig. 4d. Same as 4a for subgroup 1d

cluded from the fitting procedure. Figure 4 shows the $\log g$ vs. $\log T_{\text{eff}}$ diagrams for the four subgroups of Orion OB1, and the isochrone corresponding to the age of the subgroup.

Table 3 lists the derived ages of the subgroups, as well as the ages given by WH, and by Blaauw (1991). WH used the intrinsic colours of the bluest stars to determine the ages, by means of a technique described by Maeder (1972). WH also give an extensive review of all the age determinations done for Orion OB1 up to 1978. Many studies show that ages decrease going from 1a to 1d, but we find that 1b

is in fact younger than 1c. This agrees with the determination by de Zeeuw & Brand (1985), based on $uvby\beta$ photometry. Further support comes from the fact that subgroup 1b contains the most massive stars in Orion OB1, which are ζ Ori A ($49 M_{\odot}$), δ Ori A ($45 M_{\odot}$) and ϵ Ori A ($42 M_{\odot}$). By contrast, the most massive stars in subgroup 1c are ι Ori A ($36 M_{\odot}$) and κ Ori ($33 M_{\odot}$) (Lamers & Leitherer 1993; Vilkoviskij & Tambovtseva 1992). According to the Schaller et al. (1992) tracks, such masses put an upper limit of ~ 4 Myr on the age of subgroup 1b and a limit of ~ 5 Myr on the age of subgroup 1c. Note that also in the association Sco OB2 the subgroups are not ordered along the sky according to age. The oldest subgroup is located in between the two younger ones (GZL, de Zeeuw & Brand 1985).

Table 3. Ages of the subgroups in Myr

Subgroup	<i>VBLUW</i>	WH	Blaauw (1991)
a	11.4 ± 1.9	7.9	12
b	1.7 ± 1.1	5.1	7
c	$4.6^{+1.8}_{-2.1}$	3.7	3
d	< 1.0	< 0.5	0

Age determinations based on kinematics were made by several authors. This is usually done by tracing the projected paths of the stars backwards in time from their current position, at a constant velocity given by the observed proper motion. The time elapsed since the moment that the member stars covered the minimum extent on the sky is then taken as the *kinematic age*. In this way, Lesh (1968) derived an age of 4.5×10^6 yr ($\pm 30\%$) for subgroup 1a. Blaauw (1961) found a kinematic age of $2.2\text{--}4.9 \times 10^6$ yr for 1b, based on the motions of the three famous runaway stars, AE Aur, μ Col and 53 Ari. We return to the question of the runaway stars in section 4.5. In section 5 we discuss the ages of the subgroups in the context of sequential star formation.

4.3. Visual extinctions and the gas/dust content of the Orion region

Figure 5 is a map of the IRAS $100\mu\text{m}$ emission in the Orion region. This map is a mosaic of plates from the IRAS Sky Survey Atlas (Wheelock et al. 1993). The superimposed circles denote the positions of the programme stars. The size of a circle indicates the visual extinction A_V of the star, which is caused by foreground material. Only non-peculiar stars and binaries for which we have photometry of both components, or primaries unaffected by their companions, are included in this figure. The Orion A and B clouds and a number of well known dust/HII

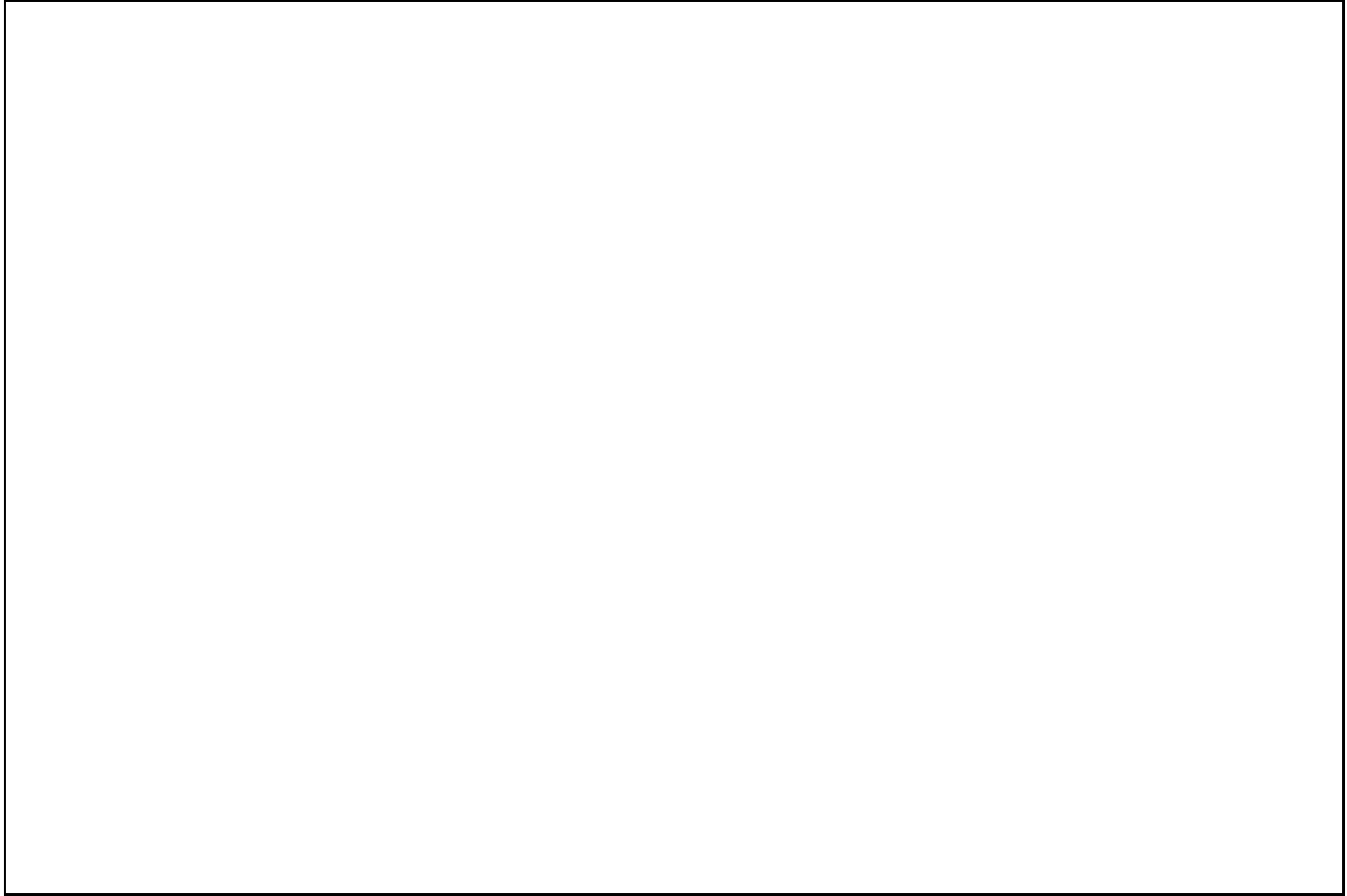


Fig. 5. Grey scale map of the IRAS 100 μm intensity in the Orion region. The lowest intensities are indicated in black and the highest are white, Galactic coordinates are used. The positions of the program stars are indicated by open circles. Their size indicates the magnitude of the visual extinction

regions are clearly outlined in this map. The Orion nebula ($\ell \approx 209^\circ, b \approx -19.5^\circ$), the Horsehead nebula, NGC 2023/NGC 2024 ($\ell \approx 206.5^\circ, b \approx -16.5^\circ$), and NGC 2064 ($\ell \approx 205.5^\circ, b \approx -14.5^\circ$) can all be seen. For the purpose of the discussion below we shall define the region where the Orion A and B clouds are located as follows. The region is enclosed between two lines. One line runs from $(\ell, b) = (217^\circ, -21^\circ)$ to $(203^\circ, -21^\circ)$ and from this last point to $(202^\circ, -12^\circ)$. The other line runs from $(\ell, b) = (217^\circ, -17^\circ)$ to $(210^\circ, -17^\circ)$ and from the last point to $(207^\circ, -12^\circ)$. A small part of the region that contains our programme stars lies within the ecliptic latitude band ($|\lambda| < 20^\circ$) where zodiacal emission contaminates the IRAS fluxes. However, the contribution of zodiacal emission is expected to be small in the 100 μm band (e.g., Beichman 1987; Rowan-Robinson et al. 1991).

Inspection of Fig. 5 reveals that the correlation between A_V and the 100 μm emission is not very tight. Many stars in the region of Orion A and B have low A_V . This can be due to: 1) the presence of small scale density enhancements, so that different lines of sight probe different dust columns, and 2) stars being at different depths in the

cloud. This second possibility suggests that we can combine the knowledge of the distances and visual extinctions to the stars with the 100 μm emission, in order to constrain the distances to and the depths of the Orion A and B clouds. Stars located in front of the molecular clouds are only reddened by foreground extinction while stars behind the clouds are also reddened by cloud material. Because A_V only measures the dust column in front of the star and the 100 μm emission measures the whole dust column along the line of sight, one expects that the values for A_V and 100 μm are essentially the same for stars behind the cloud. It follows that the distance to the near edge of the clouds can be derived from an analysis of A_V vs. distance modulus (see GZL) and the far edge can be derived from the difference between the observed 100 μm emission and that predicted by A_V (e.g., De Geus & Burton 1991).

It is difficult to apply this procedure to Orion. The Orion A and B clouds are very clumpy and filamentary, as is evident from studies in optically thin lines (Bally et al. 1987). Stars located behind the clouds may therefore have low extinction, due to the very small beam of the photometric observations. The IRAS beam, on the other hand,

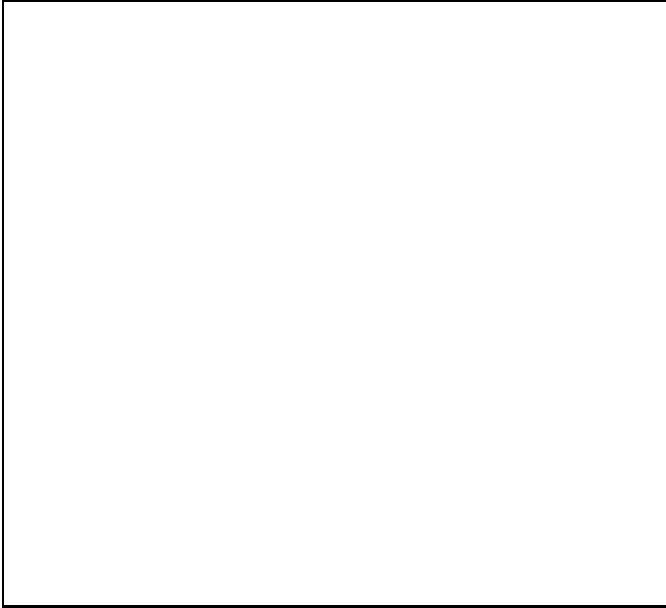


Fig. 6a. Visual extinction vs. distance modulus for all the program stars projected on the Orion A and B clouds. The line is the completeness limit for B5V stars

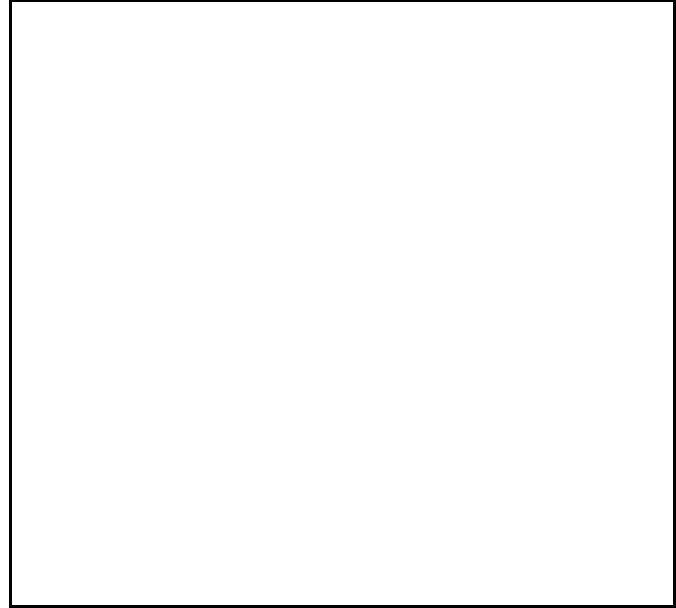


Fig. 7a. A_V vs. $100 \mu\text{m}$ intensity for the stars projected on the Orion A and B clouds. The solid line is the left-best (eye) fit to the data points as described in the text

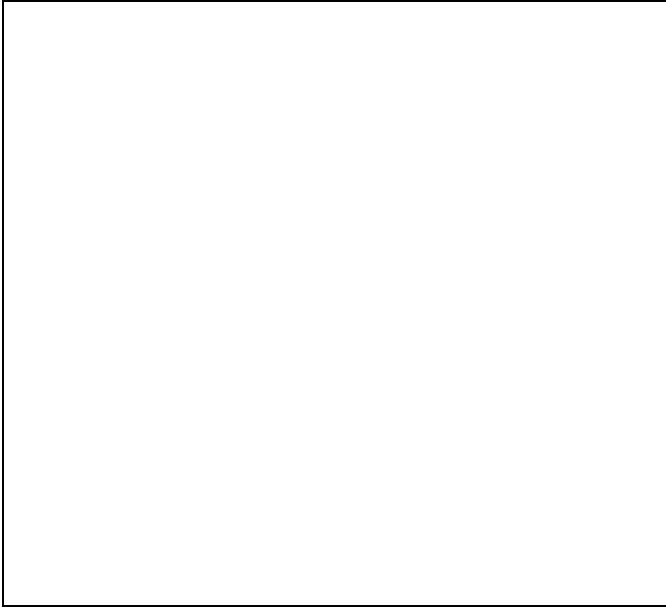


Fig. 6b. Same as 6a for stars located away from the clouds

is much larger than the photometric beam, so the $100 \mu\text{m}$ emission contains contributions from a wider dust column around the line of sight towards the star. However, if the sample of stars projected on the clouds is large enough, one might be able to constrain the distance and depth of the clouds in a statistical sense.

We divided the programme stars in two groups: stars projected on Orion A and B and stars located away from the clouds. Stars projected on the clouds are located in the area that defines Orion A and B and stars located

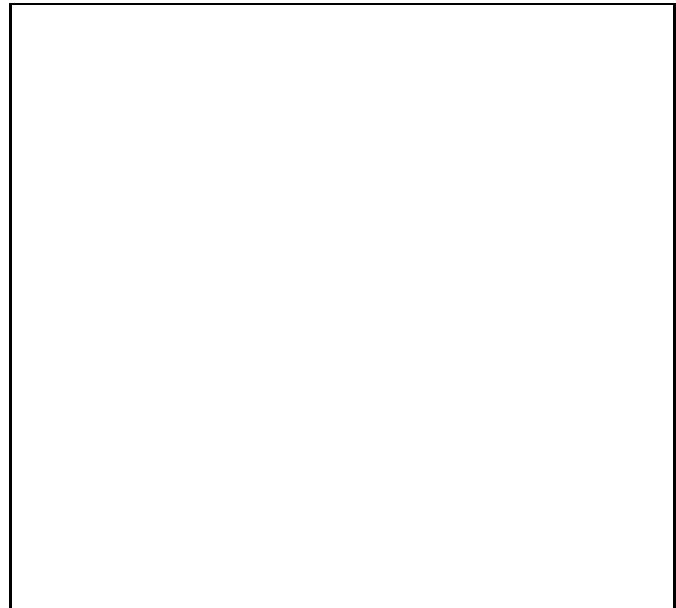


Fig. 7b. The residual component of I_{100} (corrected for the component traced by A_V) vs. the distance of the stars. The drop in the residual component at $\sim 500 \text{ pc}$ indicates the distance of the far edge of the Orion A and B clouds (see text)

away from the clouds are located at $b < -21^\circ$ and at $b < -16^\circ$ for $\ell < 203^\circ$. Table 1 indicates which stars were used in this analysis. Figures 6a and b show A_V vs. distance modulus for the two groups. The influence of the magnitude limit of the observations ($\sim 11^m$) is evident in both panels. The completeness limit for B5V stars is drawn in both plots. There is a difference between the two

groups. Stars located away from the clouds show a gradual fading out at large distance moduli. For the stars projected on Orion A and B there is a sharp limit at $\sim 9^m$. The limit is at $\sim 8^m5$ for the stars with low A_V . This suggests that we are looking into or through the cloud. From Figure 6b it is clear that there is foreground extinction at the distance of Orion OB1. Judging from the distribution of A_V values, the average foreground extinction is $\sim 0^m3-0^m4$. Therefore in order to estimate the distance of the near edge of the clouds we have to look for the distance where A_V starts to rise significantly above 0^m4 . Judging from Fig. 6a, this occurs roughly at a distance modulus of 7.5 ± 0^m5 (≈ 320 pc).

Now we turn to the far edge of the clouds. Figure 7a shows A_V vs. $100\mu\text{m}$ intensity for the stars projected on Orion A and B. The line is the left-best (eye) fit to the data and is an indication of the general relation between A_V and the $100\mu\text{m}$ emission. The line is given by:

$$I_{100} = 8 + 30A_V(\text{MJy sr}^{-1}). \quad (5)$$

This relation tells us which part of the dust column along the line of sight is measured by A_V (De Geus & Burton 1991). Subtracting the $100\mu\text{m}$ emission given by this relation from the observed emission indicates which stars lie behind the clouds. As explained above, for these stars the dust column measured by A_V should be the same as that measured by the $100\mu\text{m}$ emission. The results are shown in Fig. 7b, where the “corrected” $100\mu\text{m}$ emission is plotted vs. distance. This figure shows that the far edge of the clouds is at roughly 500 ± 30 pc. However, this is based on a small number of stars at large distances.

In conclusion, the distances to the near and far edge of the clouds are ~ 320 and ~ 500 pc, placing the clouds at a distance of 410 pc with an overall depth of approximately 180 pc. The Orion clouds span an angle of $\sim 16^\circ$ on the sky, which implies a tangential extent of roughly 120 pc. The tangential extent is consistent, within the error bars, with the depth of the clouds. An improved estimate of the depth and distance of the clouds and a possible detection of differences in distance to the various parts of the clouds requires a larger sample of stars in the direction of the clouds and the sample should include fainter stars.

4.4. Initial mass function

The mass of a star is related to $\log L/L_\odot$, $\log T_{\text{eff}}$ and $\log g$ by:

$$\log \frac{M}{M_\odot} = \log g + \log \frac{L}{L_\odot} - 4 \log T_{\text{eff}} + 10.62, \quad (6)$$

where the constant in the equation is a combination of the effective temperature and surface gravity (in cm s^{-2}) of the Sun. The derived distribution of masses in a subgroup gives the present day mass function (PDMF). The limits of the mass interval on which the PDMF is complete are

set by the maximum mass consistent with the age of the subgroup, and by the minimum mass at which the observations are complete. The initial mass function (IMF) of a subgroup was determined by fitting the PDMF on the observed mass interval to a number of functional forms $\xi(\log M)d\log M$ with the aid of a Kolmogorov-Smirnov (KS) test. The underlying assumption is that the star formation process or, conversely, the fragmentation of a molecular cloud, can be described as a stochastic process (Cayrel 1990).

In order to investigate the merits of determining the IMF with the KS-test we performed extensive Monte Carlo simulations, described in Appendix B. We find that a single power law of the form $\xi(\log M) = AM^{-B}$ with $B = 1.7 \pm 0.2$ gives an adequate description of the IMF of each of the subgroups. This IMF is consistent with the results obtained by Claudio & Grosbøl (1980), who find $B = 1.9 \pm 0.2$. Table 4 gives for each subgroup the mass interval on which the PDMF was constructed, the number of stars on this interval and the number of stars between 2 and $120 M_\odot$, according to the best fit IMF. Note, that in contrast to Blaauw (1991), we find that subgroup 1c is the richest subgroup (in number of stars) and that all the subgroups in Orion OB1 are comparable in richness to the Upper-Scorpius and Upper-Centaurus-Lupus subgroups of Sco OB2 (De Geus 1992).

Table 4. Total number of stars between 2 and $120 M_\odot$. The mass range of the PDMF and the number of stars therein is indicated

Subgroup	mass range of PDMF (M_\odot)	N_{PDMF}	N_{tot}
a	4-15	53	190
b	4-120	45	150
c	7-36	23	210

Undetected duplicity or spectral peculiarities introduce errors in the masses derived by means of Eq. (6). Not taking into account the components of multiple systems can lead to a severe underestimate of the number of observed stars contributing to the IMF in the adopted mass interval. For this reason we took masses for the known multiple stars from the literature, or we estimated them based on the magnitude difference with respect to the primary. These mass estimates were used to determine which components of a multiple system actually contribute to the PDMF in the observed mass interval. We find that the number of known multiple systems in the Orion OB1 subgroups amounts to $\approx 30\%$ of the total number of stars in our sample.

We estimated the contribution of undetected spectroscopic binaries (SB) to the PDMF by assuming that 30% of all stellar systems are SBs (e.g., Blaauw 1991). We cal-

culated a statistical correction by assuming a distribution of mass ratios as given by Hoogeveen (1992) for SB systems with a primary of spectral type B. The resulting correction for the presence of SB systems is rather small, amounting to typically 2 objects per subgroup, and can be ignored in the process of determining the IMF. The number of undetected SB systems is expected to be small because of the limited mass range on which the PDMF is determined. This means that no SB systems with secondaries of mass lower than $4 M_{\odot}$ are considered and also SBs with primaries with a mass below this limit are excluded. Peculiar stars were checked individually and if their derived masses were obviously in error compared to their spectral type, an estimate of the mass was made based on the spectral type of these stars. For subgroup 1d we did not attempt to derive an IMF because the photometry is not very reliable in this area and the observations are incomplete.

4.5. Energy output

The total energy output of an association over its lifetime is dominated by the OB stars (De Geus, 1992). To estimate the energy output of these stars, we have to distinguish the stars still present in the association from those that have already disappeared from it. For the former only the energy output through stellar winds during their main-sequence phase up to the age of the association is important. For the latter it is assumed that they have already gone through their entire evolution and have expired (or “evaporated”) as supernovae. These stars make important contributions to the energy output by the various stellar wind phases during their lifetime and by the final supernova explosion.

Massive stars experience a number of mass-loss phases during their evolution: the main-sequence or OB phase, the luminous blue variable phase, the red supergiant phase, and the Wolf-Rayet (WR) phase (Leitherer et al. 1992). The occurrence of the last three evolutionary stages, and hence their importance for the energy input into the ISM, depends on the initial mass. Leitherer et al. (1992) studied the deposition of mass, momentum and energy into the ISM by massive stars in order to apply the results to starburst galaxies. In their Fig. 3 the contributions of the four evolutionary stages to the energy deposition are shown for a model assuming an instantaneous starburst, which is appropriate for an OB association. We conclude that only the OB and the WR phases have to be considered in order to calculate the stellar wind energy output of the association.

The contributions of the OB phase were calculated by deriving the mechanical luminosity in the wind, \dot{E}_{wind} , from stellar parameters as a function of time for each star, and integrating this quantity over the main-sequence lifetime of the stars already evaporated or over the age of the association for stars still present. Due to the fact that



Fig. 8. The number of stars that have exploded as supernovae as a function of time for 1000 realizations of a synthetic association with a single power law IMF; $\xi(\log M) = AM^{-1.7}$, containing 210 stars between 2 and $120 M_{\odot}$. The solid line is the average number of supernovae, the dotted lines are the rms spreads around that average and the dashed lines represent the maximum and minimum number of supernovae that occurred

there are still O stars left in the subgroups of Orion OB1, the contributions of the stars still present are significant, in contrast to the case of, e.g., Sco OB2 (De Geus 1992).

To calculate \dot{E}_{wind} , the mass-loss rate, \dot{M} , and the terminal velocity of the wind, v_{∞} , are required. For very luminous O stars with $\log L/L_{\odot} > 5.0$ and $\log T_{\text{eff}} > 4.45$, we used the results from a recent study by Lamers & Leitherer (1993) to calculate the mass-loss rate as a function of $\log L/L_{\odot}$ and $\log T_{\text{eff}}$. The terminal velocity, v_{∞} , was calculated from the escape velocity of these stars with the aid of the simple relation, $v_{\infty}/v_{\text{esc}} = 2.8$ (Groenewegen et al. 1989). We used the “recipe” of Kudritzki et al. (1989) to derive \dot{M} and v_{∞} for late O and early B stars. Lamers & Leitherer find that this recipe predicts mass-loss rates that are on average a factor of two lower than those observed, with the precise ratio a function of the observed mean density in the wind. The predicted terminal velocities are on average a factor 1.4 larger than observed (see also Groenewegen et al. 1989). We therefore corrected the mass loss rates calculated with the Kudritzki et al. algorithm by means of Eq. (20) of Lamers & Leitherer (1993), and we multiplied the predicted terminal velocities by 0.7.

We assumed that stars with masses above $25 M_{\odot}$ go through a WR phase. We adopted an average mass-loss of $2 \times 10^{-5} M_{\odot}/\text{yr}$ in the WR phase, and a terminal velocity of $\approx 2000 \text{ km s}^{-1}$. The duration of the WR phase varies between $2.5 \times 10^5 \text{ yr}$ and $6 \times 10^5 \text{ yr}$ depending on the initial mass of the star and the mass-loss rate (Schaller et al.



Fig. 9a. Distribution of wind-energy outputs obtained in 1000 realizations of a synthetic association. The synthetic association contains the same number of stars between 2 and $120 M_{\odot}$ as subgroup 1a (Table 4) and has the same IMF. Note the long tail towards large energy outputs

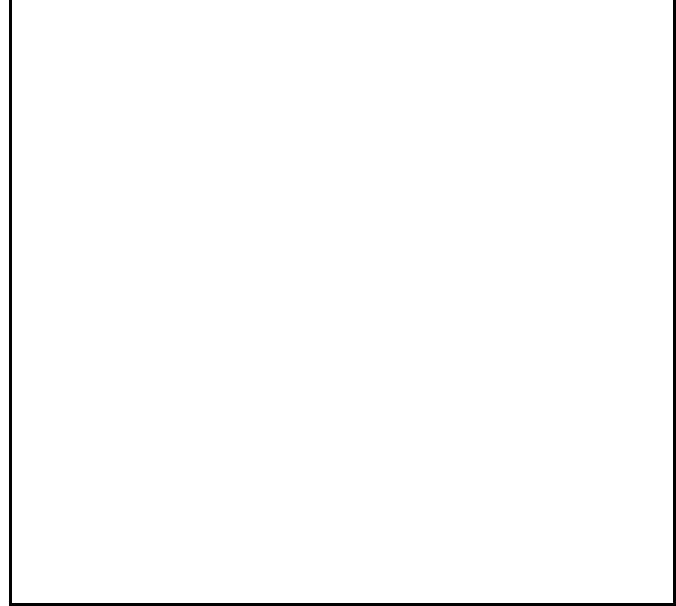


Fig. 9c. Same as 9a for the parameters of subgroup 1c

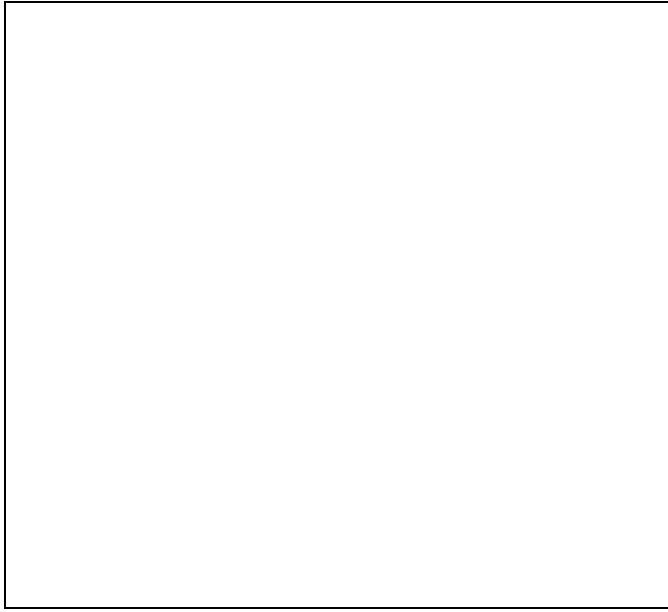


Fig. 9b. Same as 9a for the parameters of subgroup 1b

1992). For an average duration of 4×10^5 yr, each WR star contributes $3 \pm 2 \times 10^{50}$ ergs.

Finally, we assumed that each SN explosion produces 10^{51} ergs. Roughly 20% of the total energy output of an association will contribute to the kinetic energy of HI shells surrounding it (e.g., Weaver et al. 1977).

Comparison of the different contributions shows that supernovae and massive O-stars dominate the energy out-

put of the subgroups. As a result, the total energy released by the association is very sensitive to the number of massive stars that were formed or, conversely, to the upper mass cutoff in the IMF. If the process of forming an OB association with a certain IMF is viewed simply as generating a population of stars from a probability distribution given by the IMF, then the number of high mass stars will be very “noisy”. This is due to the relatively small number of stars formed in an association and the slope of the IMF.

The effects of this noise at the high mass end of the IMF were investigated with the aid of Monte Carlo simulations. We generated synthetic associations according to the power law IMF with index -1.7 that we derived for the Orion OB1 subgroups (section 4.4). We assumed the IMF to hold for the range $2-120 M_{\odot}$. The real upper mass cutoff is not known, so allowing stars up to $120 M_{\odot}$ to form will indicate the full range of possibilities.

Figure 8 shows the cumulative number of evaporated stars as a function of the age of the association, assuming 210 stars between 2 and $120 M_{\odot}$ were formed. This figure shows that the number of supernovae which occur during the early lifetime of an association has a large statistical uncertainty. The relative uncertainty is largest during the first 10 Myr; which is precisely the range relevant to this work.

The wind-energy output was calculated by combining the simulations with the calculation of wind-energies for individual stars as described above. The results are shown in Fig. 9, which gives the distribution of energy outputs for each of the three subgroups. All three distributions have a definite peak but they are very asymmetric with large tails out to high energies. These tails are caused by the fact that the total energy output from stellar winds is a

very strong function of the mass of the most massive stars that were actually formed in the subgroup. This is shown for one subgroup (1a) in Fig. 10, where the energy output is plotted vs. the mass of the most massive star in the subgroup. Even the existence of one very massive star can have a large effect on the total energy output. It follows that a simple average of the distribution of wind energies is not a good estimator of the expectation value of the total energy output. It is better in this case to take the median, which is less sensitive to tails in the distribution. The error bars will also be asymmetric.

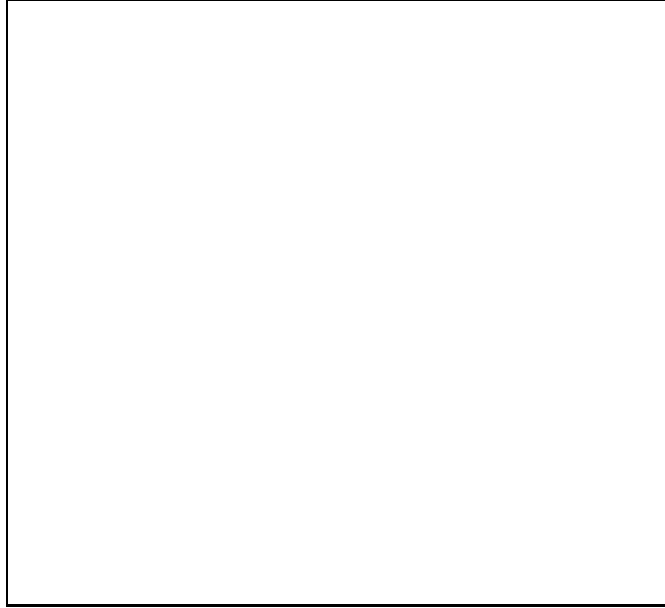


Fig. 10. Wind-energy output vs. mass of the most massive star formed for 1000 realizations of a synthetic association with parameters appropriate for subgroup 1a of Orion OB1

The energy outputs that we derive for the subgroups in Orion OB1 are shown in Table 5. In these calculations we did not take into account the fact that some stars might still be embedded in their own HII region and therefore do not contribute to the energy output of the association as a whole. This is, for instance, clearly the case for the stars in subgroup 1d. To estimate an upper limit on the magnitude of this error source we assume that a star is embedded in its own HII region throughout its main-sequence evolution. This means that we cannot count the contribution of the stellar wind of such a star in the total energy output. The most massive stars in Orion range in mass from $30-50 M_{\odot}$. Their individual energy outputs on the main sequence range from $1-3 \times 10^{50}$ ergs.

We find that with our smaller inferred age for subgroup 1b, at most two supernova events are likely to have occurred in it. There are three known runaway stars that could have originated in 1b: μ Col, AE Aur and 53 Ari. If one accepts the scenario that runaways are produced by supernova explosions in binaries (Blaauw 1961), this

Table 5. Energy outputs in 10^{50} ergs

Subgroup	SN	WR	OB	total
a	59 ± 25	7 ± 5	7_{-3}^{+11}	73_{-33}^{+40}
b	$0(< 20)$	$0(< 6)$	2_{-1}^{+8}	$2_{-1}^{+8}(< 28)$
c	14 ± 12	4 ± 4	6_{-4}^{+11}	25_{-19}^{+27}

would mean that at least three supernova events have occurred in 1b. But for the first two runaways it is not well established from which subgroup they originated and this pair could be a candidate for the dynamical ejection scenario (Gies & Bolton 1986, Leonard & Duncan 1988, 1990), because of their opposite motions, nearly equal masses, speeds and kinematic ages. The runaway 53 Ari could also have originated from 1a, in agreement with its kinematic age of 7.3 million years (see Blaauw 1991, 1993 for more details on these runaways).

5. The interaction of stars and the interstellar medium in Orion

The large scale structures in the interstellar medium around Orion OB1 have been studied extensively by means of a variety of observational techniques. Much of the early observational material was summarized by Goudis (1982). The large scale features include the Orion Molecular Cloud complex (OMC) (Maddalena et al. 1986; Kutner et al. 1977), H α emission (including Barnard's loop) which extends all the way to the Eridanus region 50° below the Galactic plane (Sivan 1974; Reynolds & Odden 1979, hereafter RO) and a hole in the neutral hydrogen distribution surrounded by H I arcs showing expanding motions (Heiles 1976; RO). The diffuse Galactic H α background intensity is enhanced in this area, and the same is true also for the X-ray intensity (e.g., RO; Burrows et al. 1993). Part of the expanding H I shell around the H I cavity was detected also by Green (1991) and Green & Padman (1993). Their H I observations extend to $\sim 35^{\circ}$ below the Galactic plane and include the Orion OB star complex. Cowie et al. (1979) measured ultraviolet absorption lines of various ionization stages of C, N, Si and S for stars in or near Orion OB1, and detected a high-velocity, low-ionization shell surrounding all of the Orion area (Orion's Cloak), as well as a dense, clumpy low-ionization shell expanding at smaller velocity. Part of this dense shell may be the negative velocity clump (in H I) described by Green & Padman (1993).

RO interpreted the various observed features as being caused by a cavity of hot ionized gas surrounded by expanding shells of H I. The ionization of the cavity is maintained by the UV radiation from the early-type stars in Orion OB1. They explained the existence of the shell as

due to a series of supernova explosions about 2×10^6 years ago. Cowie et al. interpreted the high velocity shell as the radiative shock of a supernova which occurred 3×10^5 years ago, and the high-column-density structures as the remnants of older supernova events ($2-4 \times 10^6$ years ago). Burrows et al. (1993) present a model in which the observed X-ray enhancement is due to hot gas which fills a cavity created by the stellar winds from Orion OB1.

We have shown in section 4 that the energy output from winds contributes significantly to the total energy output of the Orion OB1 association. Bally et al. (1991) presented observational evidence for ongoing interaction between the stars in Orion OB1 and its surroundings. The overall morphology of the molecular gas around Orion OB1 has a wind swept appearance (see Fig. 2 in Bally et al.), which is confirmed by several systematic patterns appearing in the morphology and kinematics of the molecular gas in Orion. Large scale velocity gradients point toward Orion OB1 and the densest parts of the molecular clouds face the association. Furthermore, the most active star formation is taking place in the dense gas closest to the OB association. In this section we investigate whether the ionized cavity containing Orion OB1 can be understood as part of an HI bubble created and maintained by the combined effect of the winds and supernovae from the association. This is followed by a discussion on sequential star formation in Orion OB1.

5.1. A simple calculation

As a first approximation for the calculation of the size and expansion velocity of the shell surrounding Orion OB1 we use the standard theory of wind-driven bubbles as given by Castor et al. (1975) and Weaver et al. (1977). McCray & Kafatos (1987) have shown that this theory can also be used for OB associations in which SN occur. We first assume spherical geometry and a uniform density ISM surrounding the HI shell. Then the shell radius R_S and expansion velocity V_S are given by (Shull 1993):

$$R_S = (26.2 \text{ pc}) L_{36}^{1/5} n_0^{-1/5} t_6^{3/5}, \quad (7)$$

$$V_S = (15.4 \text{ km s}^{-1}) L_{36}^{1/5} n_0^{-1/5} t_6^{-2/5}, \quad (8)$$

where L_{36} is the mechanical luminosity of the association averaged over its lifetime, expressed in units of $10^{36} \text{ erg s}^{-1}$, and t_6 is the age of the association in 10^6 yr . The ambient number density of the ISM is given by n_0 , and has units of cm^{-3} .

The observed radius of the HI cavity is $\sim 140 \text{ pc}$ and the expansion velocity is $15-20 \text{ km s}^{-1}$ (RO). If we take L_{36} and t_6 appropriate for Orion OB1a (20 and 11.4 respectively), and use either $n_0 = 1 \text{ cm}^{-3}$ or $n_0 = 0.1 \text{ cm}^{-3}$, then the expected size of the cavity is 210 or 330 pc, while the expansion velocity is 11 or 17 km s^{-1} . So the radius

of the HI bubble can be readily explained with the energy output of Orion OB1a alone, but the expansion velocities are too low. This estimate assumes, however, that the HI shells started expanding at the moment the stars in 1a were formed. This is not a valid approximation, as the stars have to clear their immediate surroundings (the parental molecular cloud) before their winds can influence the surrounding ISM. Not surprisingly, the dynamical age of the shells, as derived from the observed expansion velocities and size of the bubble, is 3–5 Myr. If we take this as the value for t_6 , and neglect the fact that part of the calculated energy output has gone into the disruption of the parental molecular cloud, then we find: $R_S = 120-150 \text{ pc}$, $V_S = 17-24 \text{ km s}^{-1}$ ($n_0 = 1 \text{ cm}^{-3}$) and $R_S = 190-240 \text{ pc}$, $V_S = 28-38 \text{ km s}^{-1}$ ($n_0 = 0.1 \text{ cm}^{-3}$), where L_{36} is again based on the output from subgroup 1a alone. The energy contributions from 1b and 1c will compensate for the fact that not all of the energy of 1a goes into the HI shells.

We conclude that in the spherical symmetry, constant ambient density approximation, the observed size and expansion velocities are accounted for by the stellar winds and supernovae from Orion OB1.

Note that in the model for the Orion-Eridanus bubble presented by Burrows et al. (1993) the required stellar wind luminosities are $3-10 \times 10^{36} \text{ erg s}^{-1}$, depending on the distance of the X-ray emitting gas. The stellar wind luminosities we find for the subgroups of the association ($4-7 \times 10^{36} \text{ erg s}^{-1}$) are all in this range. Thus the total stellar wind luminosity from Orion OB1 is enough to account for the observed X-ray enhancement.

5.2. The effects of a non-uniform ISM; blow out?

The assumptions of spherical symmetry and a constant ambient density clearly do not hold for Orion OB1. The star complex is located at $\sim 130 \text{ pc}$ below the Galactic plane, and we therefore have to take into account the density gradient in the HI distribution perpendicular to the plane of the Milky Way. Furthermore, the HI shells extend to $\sim 300 \text{ pc}$ below the Galactic plane, and the association is not in the center of the shells (RO; Bally et al. 1991).

No simple analytical results have been derived for the case of HI bubbles expanding in stratified media, but various numerical simulations have been performed (Mac Low & McCray 1988; Tomisaka & Ikeuchi 1986; Tenorio-Tagle & Bodenheimer 1988). These simulations show that the resulting bubbles are not spherically symmetric, but tend to be larger in the direction perpendicular to the Galactic plane. If the energy input is large enough, a “blow out” phenomenon might occur: in this case the superbubble grows in size until it breaks out of the Galactic HI layer, thereby discharging its interior energy into the Galactic halo. For energy sources not located in the plane of the Galaxy, one-sided blow out can occur.

How does the Orion-Eridanus bubble fit into this picture? The data presented in Fig. 1 of RO and the

schematic picture presented by Bally et al. (1991) show clearly that the appearance of the Orion-Eridanus bubble is in good qualitative agreement with the results of numerical simulations in which the energy source of the bubble is placed below the Galactic plane (see Figs. 5 and 8 in Mac Low & McCray 1988).

Is it possible that blow out will occur in the future? Mac Low & McCray (1988) discuss the bubble dynamics in two stratified media: an exponential distribution with a scale height of 100 pc, and a more realistic hybrid model consisting of a Gaussian cloud layer with a scale height of 135 pc and an exponential HI layer with a scale height of 500 pc (Lockman et al. 1986). The dynamical parameter that determines whether a bubble will blow out or not is the dimensionless quantity D defined as:

$$D \approx 940 L_{38} \left(\frac{H}{100 \text{ pc}} \right)^{-2} \left(\frac{P_e}{10^4 k \text{ dyne cm}^{-2}} \right)^{-3/2} n_0^{1/2}, \quad (9)$$

where L_{38} is the mechanical luminosity of the association in $10^{38} \text{ erg s}^{-1}$, H is the scale height, and P_e is the pressure of the external ISM. The value of D appropriate for Orion OB1 ranges from ~ 60 to ~ 700 , depending on the calculation of L_{38} and the assumed ambient density. Figure 6 of Mac Low & McCray shows which combinations of D and the bubble dynamical time scale result in blow-out for the case of an exponential medium. The dynamical time scale of the Orion-Eridanus bubble is 3–5 Myr, which would demand values of $D \approx 100$ for blow out. So, in this case, blow out of the Orion-Eridanus bubble may occur. The location at about 1.3 exponential scale heights from the Galactic plane also favors one-sided blow out. However, the effective scale height of the ISM is larger in the more realistic hybrid model, and as a result much higher values of D (~ 1000) are required for blow out (see also Fig. 8 in Mac Low & McCray). This suggests that the Orion-Eridanus bubble will not blow out of the Galactic HI layer.

5.3. Sequential star formation in Orion

Star formation is currently taking place in the OMC, at sites that are adjacent to the subgroups of the association. The ambient molecular gas shows signs of interaction with the Orion OB1 stars. This is indicative of sequential star formation, for which there are a number of morphological signatures. These signatures were already noted in various associations, including Orion OB1, by Blaauw (1964). They have recently been listed by Elmegreen (1992). They are: (i) regions of star formation with ages separated by several Myr and with distances between them of ~ 10 –50 pc, (ii) near the youngest subgroup there is still a substantial amount of gas and very little or no gas is left near the oldest subgroup, (iii) a velocity difference between the older and younger subgroups of ~ 5 –10 km s^{-1} , observed in either the velocities of the stars or gas or both.

In Orion OB1 all three signatures can be found. The youngest subgroup, 1d, is still closely associated with the gas (being embedded in its own HII region), while the oldest, 1a, is not associated with any gas. The distances between the four subgroups are of the order of 30–50 pc and the age differences are 3–10 Myr. No differences in radial velocity have been found so far between the subgroups (WH; Morrell & Levato 1991). The average radial velocity for the whole association is 23 km s^{-1} (Morrell & Levato 1992), whereas the bulk velocity of the gas in the Orion A and B molecular clouds is 3 – 12 km s^{-1} (Maddalena et al. 1986). A possible explanation is that the stars were formed while the gas was moving at higher velocities. The stars retained this higher velocity while the gas slowed down. The difference in present stellar and gas velocities is also related to the question of the origin of the first subgroup to which we return below.

Judging from the ages for the individual subgroups there is no linear progression of star formation from 1a to 1d. Subgroup 1c was formed before 1b and yet 1b is closer to 1a in projection, although the difference is rather small (~ 10 –20 pc). This can possibly be explained by the geometry of the system: subgroup 1c formed in a part of the OMC that was closer to 1a in the past and has since moved to its present position. At a speed of 3 – 6 km s^{-1} it could have moved the required 10–20 pc in ~ 3 Myr. Another aspect is that 1c seems more closely associated to the gas than does 1b, but this could again be a projection effect, with 1c located in front of the Orion B cloud and the HII regions in it. It is very likely that subgroups 1b and 1c are now themselves triggering star formation in various sites in the Orion A and B clouds.

Where did the oldest subgroup, 1a, come from? Several explanations have been proposed, which also involve the formation of the OMC. One possibility is that the OMC was formed as the result of the impact of a high velocity cloud (HVC) on the Galactic disk (Franco et al. 1988). The HVC approached the disk from below the Galactic plane and as a consequence of the collision a self-gravitating remnant was left which oscillated once through the Galactic plane and now constitutes the OMC. The fact that the impact took place in the south then explains the position of subgroup 1a.

Another explanation for the existence of the OMC is that it is part of the gas swept up by the expanding ring of gas known as Lindblad's ring (Lindblad et al. 1973; Olano 1982). The gas swept up in this ring was subjected to Galactic tidal forces and fragmented into a number of clouds, among which the OMC, in which star formation occurred (Elmegreen 1992, Fig. 15). The initially higher expansion velocity of the ring (Olano 1982) might be the reason why the stars in Orion OB1 move at higher radial velocities than the gas in the OMC. It is interesting to note in this context that the ages of the oldest subgroups in two other associations linked with the ring (Sco OB2 and Per OB2) are similar to the age of Orion OB1a. The existence

of the ring itself might be explained as a consequence of the deposition of energy into the ISM by the old Cas-Tau association (Elmegreen 1992; Blaauw 1991). Alternatively, the formation of the ring might be related to the origin of Gould's belt. Lindblad's ring is associated with Gould's belt (e.g., Olano 1982) and it has recently been suggested that the belt was formed as the consequence of the impact of a high velocity cloud on the galactic disk (Comerón & Torra 1992). Such an impact could also lead to the formation of Lindblad's ring (e.g., Elmegreen 1992).

We conclude that past geometries of the system of stars and gas can explain our finding that subgroup 1b is younger than 1c. The formation of 1a might be the consequence of the impact of a high velocity cloud on the Galactic disk or it might have formed when the expanding Lindblad ring fragmented into molecular clouds.

6. Conclusions and future work

We derived physical parameters for candidate members of the Orion OB1 association, based on *VBLUW* photometry. Distances to the stars and the subgroups of the association were calculated and it was shown that in subgroup 1b there is no increase in distance from west to east. New photometric members of Orion OB1 were identified based on the distances to the subgroups and the rms spreads in them, calculated from the distances of known members.

Ages were derived for all the subgroups by fitting isochrones in the $\log T_{\text{eff}}$, $\log g$ plane. This method of age determination suffers from the small number of stars at the main-sequence turnoff in an association and the large errors in $\log g$. Extensive simulations were performed to investigate the influence of these error sources on the age determination and in order to choose the best fitting method (appendix A). The results show that subgroup 1b is not intermediate in age between 1a and 1c, as is often assumed, but is in fact the younger of the three, so that the sequence of increasing age is: 1d, 1b, 1c, 1a.

Visual extinctions derived for all programme stars were compared to IRAS 100 μm skyflux data in order to constrain the distances and depths of the GMCs Orion A and B. We find that the near edge of the Orion A and B clouds is located at a distance of ~ 320 pc and the far edge of the clouds is at ~ 500 pc.

Simulations show that with the limited amount of data available on the PDMF of the subgroups in Orion OB1 it is very difficult to constrain the IMF accurately (appendix B). A stellar IMF of the form $\xi(\log M) = AM^{-B}$ fits the observations of each of the subgroups 1a, 1b and 1c. In all three cases the exponent B is 1.7 ± 0.2 . The stellar content, the ages and the IMF of the subgroups were combined to calculate the amount of energy that was released into the ISM by Orion OB1. These energies are sufficient to account for the Orion-Eridanus bubble; blow out of this bubble may occur, but this depends critically on the z-distribution of the surrounding gas.

Orion OB1 displays many indications of sequential star formation. We speculate that past geometries of the system of gas and stars can explain our finding that subgroup 1b is younger than 1c. Two possible scenarios for the origin of the oldest subgroup (1a) were discussed. The formation of 1a might be the consequence of the impact of a high velocity cloud in the Galactic disk or it might have formed when the expanding Lindblad ring fragmented into molecular clouds. At present, we cannot distinguish between these two alternatives.

Future work includes an analysis of the HIPPARCOS data together with radial velocities obtained as part of an ESO Key Programme (Hensberge et al. 1990). This will provide improved membership lists and possibly the internal motions in Orion OB1. Another interesting project is to take a more detailed look at the ISM in the vicinity of Orion OB1. This can be done by combining the new HI data of Hartmann & Burton (1993) with existing CO and IRAS data. In this way different components of the ISM can be studied and this will allow a more detailed analysis of the extinctions (see section 4.3), as well as a more refined analysis of the interaction of the stars and the ISM. Work along these lines is in progress.

Acknowledgements. It is a pleasure to thank A. Blaauw and H. Lamers for stimulating discussions. We thank T. Chester and S. Wheelock for providing the IRAS Sky Survey plates and D. Kester for help with producing the mosaic of these plates. We are grateful to the referee, J. Hesser, for a meticulous reading of the manuscript. This research was supported (in part) by the Netherlands Foundation for Research in Astronomy (NFRA) with financial aid from the Netherlands organization for scientific research (NWO). EdG acknowledges support from NSF grant AST-8918912 and NASA grant NAG5-1736.

Appendix A: age determination

The ages of the subgroups in Orion OB1 were derived by fitting theoretical isochrones to the observational data in the $\log g$, $\log T_{\text{eff}}$ plane. The age of a subgroup was determined by minimizing:

$$\Psi^2 = \sum_{i=1}^N d_{\min,i}^2 W_i \quad (1),$$

where $d_{\min,i}$ is the shortest distance from the isochrone to the data point i and W_i is a weight factor, which is different for each star. This method suffers from a number of problems:

- Accidental errors in $\log g$ are large ($\sigma(\log g) \approx 0.25$ for $\log T_{\text{eff}} > 4.3$ and $\sigma(\log g) \approx 0.1$ for $\log T_{\text{eff}} < 4.3$);
- Due to the steep slope of the IMF there is only a small number of stars at the turnoff of the isochrone;

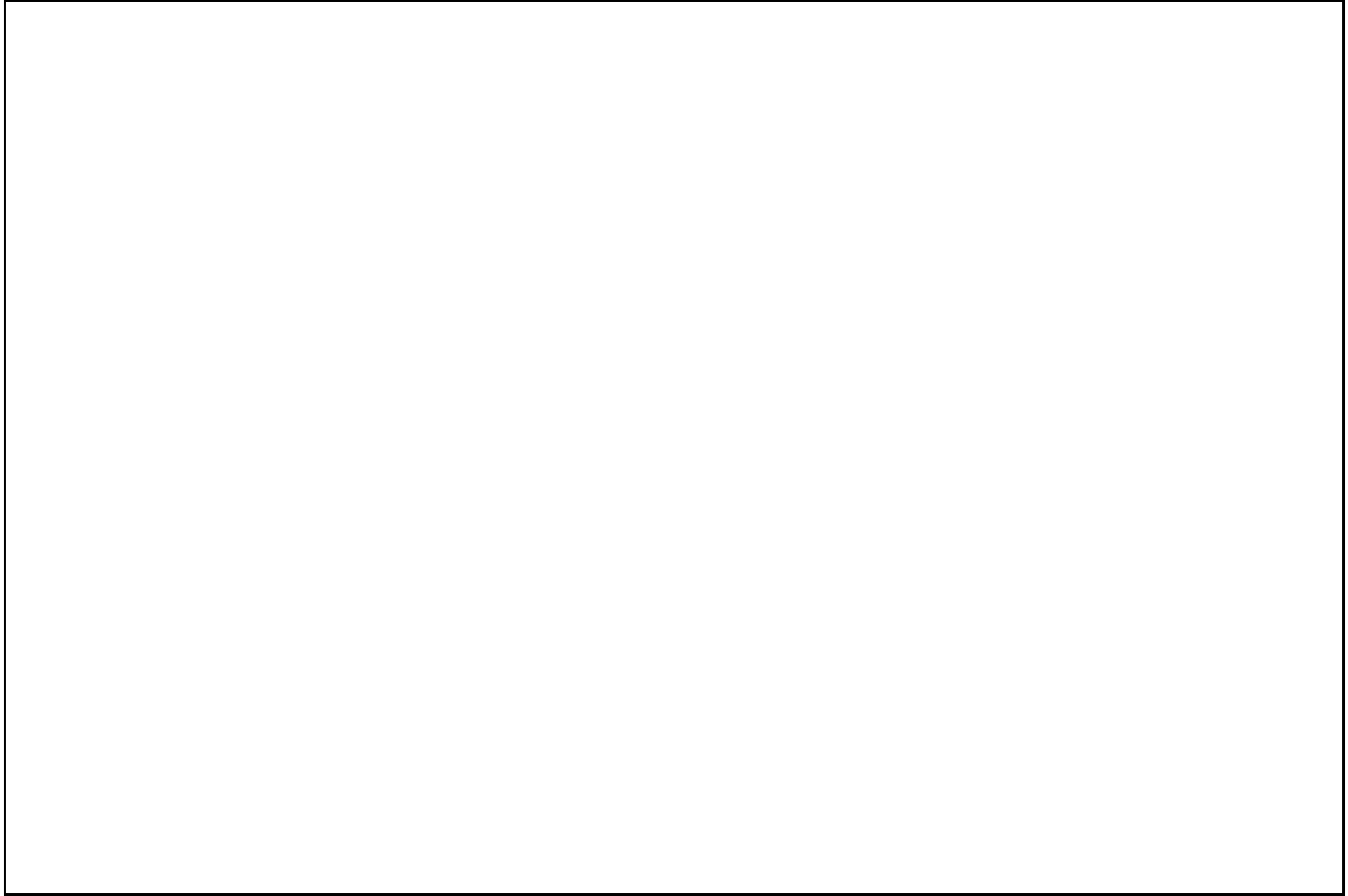


Fig. 11. Hertzsprung-Russell diagram of $\log g$ vs. $\log T_{\text{eff}}$ with the Kurucz grid drawn in. Solid lines are theoretical stellar evolution tracks and the dashed lines are isochrones for 1, 3, 5, 10, 15, 25 and 50 Myr. The ZAMS is indicated with a solid line

- Due to the binary or peculiar nature of some stars $\log g$ and $\log T_{\text{eff}}$ may be in error;
- Contamination by non-members.

We performed Monte Carlo simulations in order to assess how well the fitting method works, and to investigate the effects of the relatively large errors in $\log g$ and the influence of the slope of the IMF. We generated synthetic associations by drawing a population of stars from a distribution which has the same form as the IMF. The association was aged with the aid of the theoretical evolutionary tracks and the parameters of the stars in the association were transformed to the $\log g$, $\log T_{\text{eff}}$ plane. Random (normally distributed) observational errors were added in accordance with the errors of our observations (section 3). Figure 11 shows the theoretical evolutionary tracks that we used. The Kurucz grid is also plotted in this figure to illustrate that at the high mass end the isochrones cannot be transformed to the $[B - U]$ vs. $[B - L]$ diagram. Figure 12 shows an example of a synthetic association in the $\log g$, $\log T_{\text{eff}}$ plane, together with the isochrone representing its real age.

The synthetic associations do not contain any binaries; the occurrence of non-members in the data was also not

taken into account. Undetected binaries may give rise to erroneous points in the $\log g$, $\log T_{\text{eff}}$ plane, as the measured colours are for the composite light rather than for the individual components. In practice this effect is not very important. For a large fraction of the binaries we obtained photometry for both components, and the bulk of the remainder has a companion of a mass too low to influence the colours. In cases where there are doubts about the colours of a star because its companion is also in the diaphragm of the photometer and is bright enough to influence the colours, the data were simply excluded from the actual fitting process. Non-members, i.e., interlopers, generally increase the number of low-mass stars and this often leads to gross overestimates of the age of an association. To prevent this, stars with $\log T_{\text{eff}} < 4.15$ were excluded from the fitting process. This temperature was chosen because below this value isochrones for less than 50 Myr become practically indistinguishable to the fitting process (see Fig. 11).

Many realizations of a synthetic association were calculated for different ages, and we fitted theoretical isochrones for each of them according to the procedure mentioned above. The results were analyzed for three effects:



Fig. 12. Hertzsprung-Russell diagram of $\log g$ vs. $\log T_{\text{eff}}$ for a synthetic association containing 300 stars with masses between 2 and $120 M_{\odot}$. The association has a single power law IMF: $\xi(\log M) = AM^{-1.6}$ and its age is 5 Myr. The solid line is the isochrone that corresponds to the age of the association. Note the influence of the large errors in $\log g$ at high temperatures (the region of the main sequence turn off)

- What should the choice be for the weights W in Eq. (1)?
- What is the influence of the functional form of the IMF?
- What accuracies in $\log g$ (and $\log T_{\text{eff}}$) are required for accurate age determinations?

A weight factor W is introduced in Eq. (1) to compensate for the fact that there are only a few stars at the high-mass end of the IMF compared to the number of low-mass stars. This means that without weighting, the stars at the main-sequence turnoff will effectively play no role in the age determination. Yet, the turnoff contains all the information. The obvious choice for W would be some power of the stellar mass, so as to compensate for the shape of the IMF. But stellar masses contain the errors in $\log T_{\text{eff}}$, $\log g$ and M_{bol} and are thus very uncertain.

After some experimentation we found that a good way of assigning weights is to use $W = \log T_{\text{eff}}$. The errors in $\log T_{\text{eff}}$ are relatively small and it is a physical parameter which follows from the observations, thus removing the arbitrariness that plagues many other weighting schemes. Figures 13a and b show the average age determined by isochrone fitting as a function of the real age, for two different IMFs (single power law and the Miller & Scalo form – see below). For each age plotted, 1000 simulations were used. The error bars indicate the rms spreads in the derived ages, and vary between 0.9 and 2.4 Myr. There clearly is a smooth correlation between the estimated and



Fig. 13a. Best estimate of the age (which follows from isochrone fitting) vs. the real age of the association. The results for each age are the average of 1000 simulations. The error bars indicate rms spreads. The results are shown for a synthetic association that contains 300 stars between 2 and $120 M_{\odot}$ and the IMF is: $\xi(\log M) = AM^{-1.6}$

the real ages. The derived ages are systematically overestimated, but a second degree polynomial can be fitted quite satisfactorily to the results with a χ^2 of 0.02 and 0.05 and average residuals 0.06 and 0.1, for the single power law and the Miller & Scalo IMF, respectively. This relation can then be used to correct ages derived for observed associations.

A disadvantage of the $\log T_{\text{eff}}$ weighting scheme is that stars at the turnoff on isochrones of low age can get the same weights assigned even though their masses are different. This is probably also part of the cause of the systematic overestimate of the derived ages (the other part is probably the relatively high number of low mass stars). In order to check whether this problem can be resolved we also tested a weighting scheme which is a combination of $\log g$ and $\log T_{\text{eff}}$. This would remove the problems with the $\log T_{\text{eff}}$ weights at the high mass end. We tried a scheme with weights T^4/g which is basically L/M , a quantity that increases steeply with mass. This scheme also results in a smooth trend in derived age vs. real age, but it is less smooth than that obtained with the simple $\log T_{\text{eff}}$ weights, and higher order polynomials or more complicated functions are needed to fit the relation. The ages quoted in section 4.2 were derived with the $\log T_{\text{eff}}$ weighting scheme.

The second question that can be answered with the results of the simulations is whether the shape of the IMF makes any difference in deriving ages. Again, the most important influence of the IMF is that there are only a

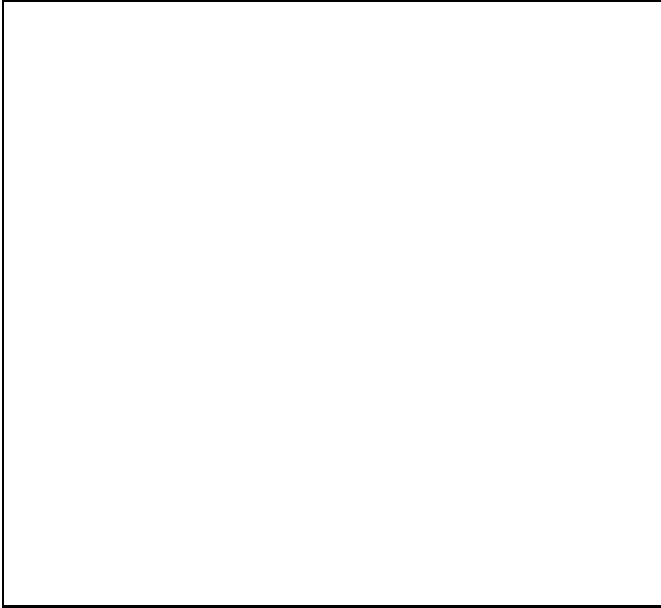


Fig. 13b. The same as 13a for an association containing the same number of stars, but following a Miller & Scalo IMF

few stars at the main-sequence turnoff for young associations. Moreover, an IMF with a steeper slope at the high mass end might make it more difficult to determine correct ages. We tried two different IMFs, a single power law: $\xi(\log M) = AM^{-1.6}$ (see e.g., Basu & Rana 1992); and a Miller & Scalo IMF: $\xi(\log M) = AM^{-B}$, where $B = 0.4$ for $M < 1 M_\odot$, $B = 1.5$ for $1 < M < 10 M_\odot$ and $B = 2.1$ for $M > 10 M_\odot$ (see De Geus 1992). The results for the two IMFs look similar as shown in Figs. 13a and b, and the derived ages are all consistent within the rms spreads, although for ages below ~ 5 Myr the single power law IMF results in somewhat smaller overestimates. Also, when correcting the derived age to the real age, the results for the two IMFs are entirely consistent within the error bars.

The fact that the difference in the IMFs cannot be seen in the results implies that the age determinations are dominated by the observational errors in $\log g$ and $\log T_{\text{eff}}$. The simulations were repeated with lower observational errors and it turns out that if the observational errors, and in particular those in $\log g$, were a factor of three smaller, then the ages can be derived with an accuracy of ± 0.5 Myr. This translates to requiring that bolometric magnitudes be determined with errors less than 0.2–0.4 magnitudes. Improvements in the absolute magnitude calibration can be expected when HIPPARCOS data become available for nearby early-type stars.

Appendix B: the initial mass function

There are a number of ways to determine the stellar IMF for a group of stars. The conventional approach is to plot the number of stars as a function of mass in a log-log diagram and fit a power law IMF to the data. But if the star

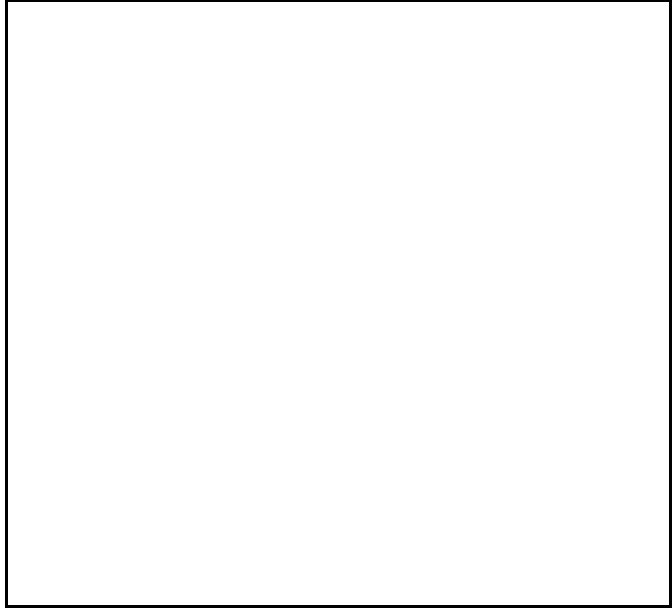


Fig. 14a. Mean (from 1000 simulations) of the probability (P) that the synthetic association, generated according to a Miller & Scalo IMF, has the single power law IMF that is indicated on the abscissa (by its power law index). The square indicates that the mass distribution was compared to a Miller & Scalo IMF. Parameters of the synthetic association are indicated

formation process is viewed as drawing a population of stars randomly from a distribution function of the same form as the IMF (see section 4.4), the conventional approach is not the right method. In such a procedure, fitting a power law to the observations does not take into account that a particular population of stars drawn from the IMF does not necessarily reflect the underlying distribution of masses accurately.

The statistical test that can be applied to check whether an observed population could have been drawn from a certain distribution is the Kolmogorov-Smirnov test. The procedure in this case is to determine first the present day mass function (PDMF), and compare it to assumed forms of the IMF with the aid of the KS-test. However,

- The PDMF is known completely only in a limited mass interval, with the limits being set by the minimum mass at which the observations are complete and by the maximum mass which follows from the age of the subgroup;
- The number of stars in this interval is limited: 20 to 50 stars in the case of the Orion OB1 subgroups;
- For high mass stars ($M \gtrsim 10 M_\odot$) there are large uncertainties in the masses, caused by the large errors in $\log g$ (see also section 3).

We performed Monte Carlo simulations in order to investigate how well the KS-test can distinguish between different forms of the IMF. As in Appendix A, this was

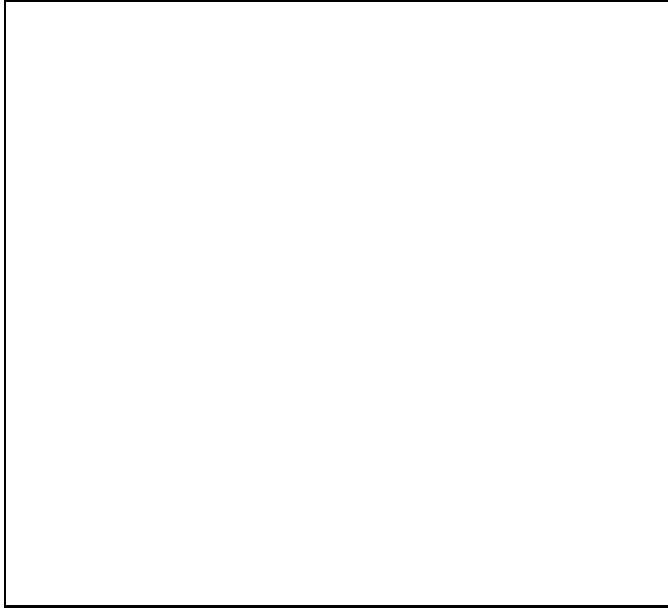


Fig. 14b. Same as 14a for a synthetic association generated according to a single power law IMF

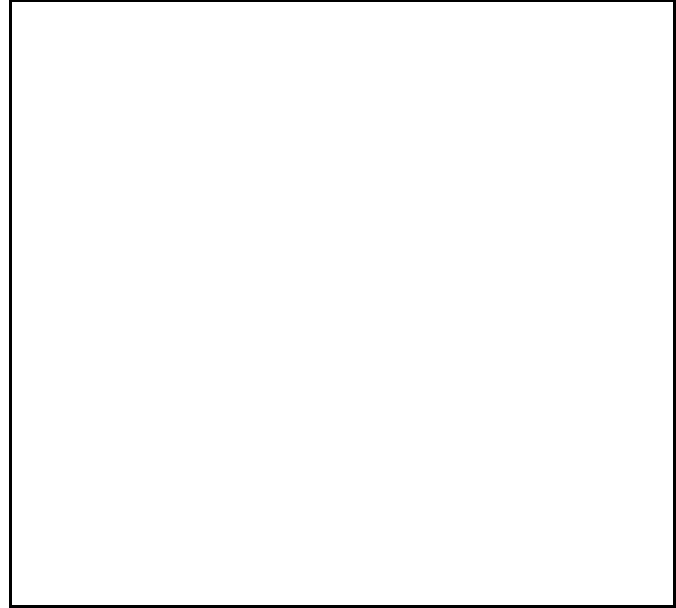


Fig. 15b. Same as 15a for subgroup 1b

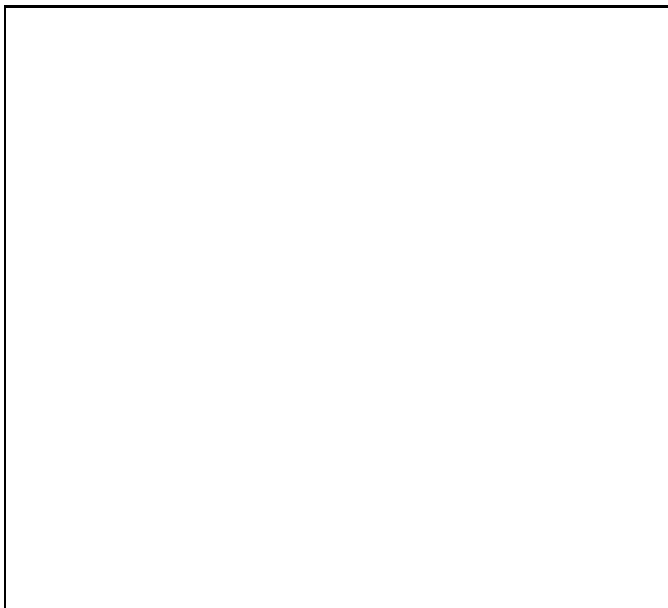


Fig. 15a. The same as Fig. 14, but now the results obtained when applying the KS-test to the actual present day mass function of subgroup 1a are shown. The parameters of the PDMF are listed in Table 4

done by generating synthetic associations according to the IMF and applying the KS-test on a limited mass interval ($4-30 M_{\odot}$) with a number of stars similar to what is seen in Orion OB1. The PDMF of the synthetic association was compared to a range of single power law IMFs (indices varying from -0.4 to -2.1) and to the Miller & Scalo IMF (see Appendix A). The synthetic associations had a single power law IMF (index -1.6) or the Miller



Fig. 15c. Same as 15a for subgroup 1c

& Scalo IMF. The results are shown in Fig. 14 where the mean of the probability that the PDMF is drawn from the IMF is plotted against the form of the comparison IMF. We used 1000 realizations of the synthetic association. We conclude:

- Based on the small number of observations it is nearly impossible to distinguish between different single power law IMFs (although the diagrams might look better in individual cases).
- A single power law IMF with an index close to -1.5 cannot be distinguished from a Miller & Scalo IMF

and vice versa, which is partly due to the limited mass range over which we fit the PDMF to the IMF.

From Fig. 14 it is evident that the error bars on the power law index of the IMF are rather large. In fact, if one were to be conservative and demand a confidence level of 95% for the derived index, then almost every IMF is consistent with the data. Again, a better determination may be possible in individual cases. The simulations showed that the error bars on the index are much smaller if the PDMF contains the data of ~ 100 stars or more.

Figure 15 shows the results for the Orion OB1 subgroups. For subgroup 1a, the IMF that is most consistent with the observations is the single power law IMF with power law index -1.7 , but, demanding a confidence level of 70%, all single power law IMFs with indices between -1.3 and -2.1 and the Miller & Scalo IMF are consistent with the observations. Similarly, for subgroup 1b the index is -1.6 , with indices -1.2 to -1.9 and the Miller & Scalo IMF being consistent at the 70% confidence level. In the case of subgroup 1c (note the effect of the very low number of stars), -1.7 is the most consistent index, with indices between -1.0 and -2.1 and the Miller & Scalo IMF being consistent with the data at the 70% confidence level. Taking into account the large error bars, we adopt a single power law IMF with index -1.7 for all three subgroups.

References

van Altena, W.F., Lee, J.T., Lee, J.-F., Lu, P.K., Upgren, A.R., 1988, AJ 95, 1744

Anthony-Twarog, B.J., 1982, AJ 87, 1213

Bally, J., Langer, W.D., Stark, A.A., Wilson, R.W., 1987, ApJ 312, L45

Bally, J., Langer, W.D., Wilson, R.W., Stark, A.A., Pound, M.W., 1991, Fragmentation of Molecular Clouds and Star Formation, IAU Symp. 147, eds. E. Falgarone, F. Boulanger & G. Duvert (Dordrecht: Kluwer), p. 11

Bastian, U., Röser, S., Nesterov, V.V. et al., 1991, A&AS 87, 159

Basu, S., Rana, N.C., 1992, ApJ 393, 373

Beichman, C.A., 1987, ARA&A 25, 521

Blaauw, A., 1961, Bull. Astr. Inst. Netherlands 15, 265

Blaauw, A., 1964, ARA&A 2, 213

Blaauw, A., 1991, in The Physics of Star Formation and Early Stellar Evolution, eds. C.J. Lada & N.D. Kylafis, NATO ASI Series C, Vol. 342, p. 125

Blaauw, A., 1993, in Massive Stars: Their Lives in The Interstellar Medium, eds. J.P. Casinelli & E.B. Churchwell, ASP conference series, Vol. 35, p. 207

Brand, J., Wouterloot, J.G.A., 1988, A&AS 75, 117

Burrows, D.N., Singh, K.P., Nousek, J.A., Garmire, G.P., Good, J., 1993, ApJ 406, 97

Castor, J., McCray, R., Weaver, R., 1975, ApJ 200, L107

Cayrel, R., 1990, in Physical Processes in Fragmentation and Star Formation, eds. R. Capuzzo-Dolcetta, C. Chiosi & A. Di Fazio, p. 343

Claudius, M., Grosbøl, P.J., 1980, A&A 87, 339

Chromey, F.R., Elmegreen, B.G., Elmegreen, D.M., 1989, AJ 98, 2203

Comerón, F., Torra, J., 1992, A&A 261, 94

Cowie, L.L., Songaila, A., York, D.G., 1979, ApJ 230, 469

Crawford, D.L., 1978, AJ 83, 48

Crawford, D.L., Barnes, J.V., 1966, AJ 71, 610

Elmegreen, B.G., 1992, in Star Formation in Stellar Systems, eds. G. Tenorio-Tagle, M. Prieto & F. Sánchez, Cambridge University Press, p. 383

Elmegreen, B.G., Lada, C.J., 1977, ApJ 214, 725

Franco, J., Tenorio-Tagle, G., Bodenheimer, P., Rózycka, M., Mirabel, I.F., 1988, ApJ 333, 826

de Geus, E.J., 1991, in The Formation and Evolution of Star Clusters, ed. K. Janes, ASP conference series, Vol. 13, p. 40

de Geus, E.J., 1992, A&A 262, 258

de Geus, E.J., Burton, W.B., 1991, A&A 246, 559

de Geus, E.J., de Zeeuw, P.T., Lub, J. (GZL), 1989, A&A 216, 44

de Geus, E.J., Lub, J., van de Grift, E., 1990, A&AS 85, 915

Genzel, R., Stutzki, J., 1989, ARA&A 27, 41

Gies, D.R., Bolton, C.T., 1986, ApJS 61, 419

Groenewegen, M.A.T., Lamers, H.J.G.L.M., Pauldrach, A. W.A., 1989, A&A 221, 78

Goudis, C., 1982, The Orion Complex: A Case Study of Interstellar Matter, Astrophys. Space Sci. Libr., Vol. 90, Dordrecht: Reidel

Green, D.A., 1991, MNRAS 253, 350

Green, D.A., Padman, R., 1993, MNRAS 263, 535

Hardie, R.H., Heiser, A.M., Tolbert, C.R., 1964, ApJ 140, 1472

Hartmann, D., Burton, W.B., 1994, in preparation

Heiles, C., 1976, ApJ 208, L137

Hensberge, H., van Dessel, E.L., Burger, M. et al., 1990, The Messenger, 61, 20

Hoogeveen, S.J., 1992, Ap&SS 196, 299

Jones, B.F., Walker, M.F., 1988, AJ 95, 1755

Jung, J., Bischoff, M., 1971, Bulletin d'Information du Centre de Donnees Stellaires 2, 8

Kudritzki, R.P., Pauldrach, A., Puls, J., Abbott, D.C., 1989, A&A 219, 205

Kurucz, R.L., 1979, ApJS 40, 1

Kutner, M.L., Tucker, K.D., Chin, G., Thaddeus, P., 1977, ApJ 215, 521

Lada, E.A., Bally, J., Stark, A.A., 1991, ApJ 368, 432

Lamers, H.J.G.L.M., Leitherer, C., 1993, ApJ 412, 771

Lesh, J.R., 1968, ApJ 152, 905

Leitherer, C., Robert, C., Drissen, L., 1992, ApJ 401, 596

Leonard, P.J.T., Duncan, M.J., 1988, AJ 96, 222

Leonard, P.J.T., Duncan, M.J., 1990, AJ 99, 608

Lindblad, P.O., Grape, K., Sandqvist, Aa., Schober, J., 1973, A&A 24, 309

Lub, J., Pel, J.W., 1977, A&A 54, 137

Lockman, F.J., Hobbs, L.M., Shull, J.M., 1986, ApJ 301, 380

Mac Low, M.-M., McCray, R., 1988, ApJ 324, 776

Maddalena, R.J., Morris, M., Moscowitz, J., Thaddeus, P., 1986, ApJ 303, 375

Maeder, A., 1972, in IAU Colloquium No. 17, Stellar Ages, eds. G. Cayrel de Strobel & A.M. Delplace (Meudon: Observatoire de Paris), §XXIV

McCray, R., Kafatos, M.C., 1987, ApJ 317, 190

Miller, G.E., Scalo, J.M., 1979, ApJS 41, 513

Morgan, W.W., Lodén, K., 1966, Vistas in Astronomy 8, 83

Morrell, N., Levato, H., 1991, ApJS 75, 965

Olano, C.A., 1982, A&A , 112, 195

Parenago, P.P., 1953, AZh. 30, 249 (English Trans. in Astr. Newsletter 74, 20)

Parenago, P.P., 1954, Publ. Sternberg Astron. Inst. No. 25

Reynolds, R.J., Ogden, P.M., 1979, ApJ 229, 942

Röser, S., Bastian, U., 1989, PPM-postions and proper motions of 181731 stars north of -2.5 degrees declination, Astron. Rechen-Inst. Heidelberg.

Rowan-Robinson, M., Hughes, J., Jones, M. et al., 1991, MNRAS 249, 729

Schaller, G., Schaerer, D., Meynet, G., Maeder, A., 1992, A&AS , 96, 269

Sharpless, S., 1952, ApJ 116, 251

Sharpless, S., 1962, ApJ 136, 767

Shull, J.M., 1993, in Massive Stars: Their Lives in the Interstellar Medium, eds. J.P. Casinelli & E.B. Churchwell, ASP conference series Vol. 35, p. 327

Sivan, J.P., 1974, A&AS 16, 163

Smart, R.L., 1993, PhD. thesis University of Florida

Straizys, V., Kuriliene, G., 1981, Ap&SS 80, 353

Strand, K.Aa., 1958, ApJ 128, 14

Tenorio-Tagle, G., Bodenheimer, P., 1988, ARA&A 26, 145

Tomisaka, K., Ikeuchi, S., 1986, PASJ 38, 697

Turon, C., Crézé, M., Egret, D. et al., 1992, ESA SP-1136

Vilkoviskij, E.Ya., Tambovtseva, L.V., 1992, A&AS 94, 109

Walker, M.F., 1969, ApJ 155, 447

Warren, W.H., Hesser, J.E., 1977 (WH), ApJS 34, 115

Warren, W.H., Hesser, J.E., 1978 (WH), ApJS 36, 497

Weaver, R., McCray, R., Castor, J., Shapiro, P., Moore, R., 1977, ApJ 218, 377 (err 220, 742)

Wheelock, S. et al., 1993, IRAS Sky Survey Atlas Explanatory Supplement

de Zeeuw, P.T., Brand, J., 1985, in Birth and Evolution of Massive Stars and Stellar Groups, eds. W. Boland & H. van Woerden, Dordrecht: Reidel, p. 95

This article was processed by the author using Springer-Verlag T_{EX} A&A macro package 1992.